Check for updates

ADVANCING EARTH AND SPACE SCIENCES

JGR Atmospheres

RESEARCH ARTICLE

10.1029/2024JD041138

The Cumulative Effect of Wintertime Weather Systems on the Ocean Mixed-Layer Stable Isotope Composition in the Iceland and Greenland Seas

Harald Sodemann[1,2], Yongbiao Weng[1,2], Alexandra Touzeau[1,2], Emil Jeansson[2,3], Iris Thurnherr[1,2], Chris Barrell[4], Ian A. Renfrew[4], Stefanie Semper[1,2], Kjetil Våge[1,2], and Martin Werner[5]

[1]Geophysical Institute, University of Bergen, Bergen, Norway, [2]Bjerknes Centre for Climate Research, Bergen, Norway, [3]NORCE Norwegian Research Centre, Bergen, Norway, [4]Centre for Ocean and Atmospheric Sciences, School of Environmental Sciences, University of East Anglia, Norwich, UK, [5]Alfred Wegener Institute Helmholtz Centre for Polar and Marine Research, Bremerhaven, Germany

Key Points:

- We observe pronounced variability in the stable isotope composition of the atmosphere-ocean system during winter
- Vapor and precipitation isotope variations reflect local and remote factors associated with different weather systems
- We find indications that weather systems can leave a cumulative d-excess imprint in the ocean mixed layer

Supporting Information:

Supporting Information may be found in the online version of this article.

Correspondence to:

H. Sodemann,
harald.sodemann@uib.no

Citation:

Sodemann, H., Weng, Y., Touzeau, A., Jeansson, E., Thurnherr, I., Barrell, C., et al. (2024). The cumulative effect of wintertime weather systems on the ocean mixed-layer stable isotope composition in the Iceland and Greenland Seas. *Journal of Geophysical Research: Atmospheres*, *129*, e2024JD041138. https://doi.org/10.1029/2024JD041138

Received 21 MAR 2024
Accepted 17 SEP 2024

Author Contributions:

Conceptualization: Harald Sodemann, Ian A. Renfrew
Data curation: Harald Sodemann
Formal analysis: Yongbiao Weng, Alexandra Touzeau, Emil Jeansson, Iris Thurnherr, Chris Barrell
Funding acquisition: Harald Sodemann
Investigation: Harald Sodemann, Yongbiao Weng, Alexandra Touzeau, Emil Jeansson, Iris Thurnherr, Stefanie Semper
Methodology: Harald Sodemann, Yongbiao Weng, Alexandra Touzeau, Iris Thurnherr, Chris Barrell, Stefanie Semper, Martin Werner

© 2024. The Author(s).
This is an open access article under the terms of the Creative Commons Attribution License, which permits use, distribution and reproduction in any medium, provided the original work is properly cited.

Abstract The Iceland and Greenland Seas are characterized by strong heat fluxes from the ocean to the atmosphere during wintertime. Here we characterize the atmospheric signal of this strong evaporation in terms of water vapor isotopes and investigate if such a signal can have a cumulative imprint on the ocean mixed-layer. Observations include continuous water vapor isotope measurements, event-based precipitation samples, and sea-water samples taken at various depths from the research vessel Alliance during the Iceland-Greenland Seas Project cruise in February and March 2018. In conjunction with a simulation from a regional, isotope-enabled atmospheric model, we find that the predominant atmospheric isotope signature during predominant marine cold-air outbreak conditions is $-129.8 \pm 16.6‰$ for δ^2H and $-18.10 \pm 2.87‰$ for $\delta^{18}O$, with a d-excess of $15.1 \pm 7.9‰$, indicating enhanced non-equilibrium fractionation compared to the global average. During events of warm-air intrusion from mid-latitudes, near-surface vapor becomes saturated and the vapor d-excess approaches equilibrium or becomes negative. Similarly, precipitation d-excess is lower and thus closer to equilibrium conditions during warm-air intrusions. There are indications that an evaporation signal of waters exiting the Nordic Seas through Denmark Strait could be locally enhanced over seasons to years, as supported by simple model calculations. Our findings thus suggest that evaporation signals could be transferred into the ocean isotope composition in this region, potentially enabling mass-balance constraints in isotope-enabled coupled ocean-atmosphere models.

Plain Language Summary The sea area between Iceland, Greenland, and Fram Strait experiences strongly variable weather conditions during wintertime. Often, cold air sweeps over open waters, leading to intense extraction of heat and water from the ocean. Also opposite conditions can occur, where air from warmer and more humid mid-latitudes extends northward, reaches saturation, and loses heat to the underlying surface. During the Iceland-Greenland Seas Project cruise in February and March 2018, we measured the stable water isotope composition in water vapor, snow, rain, and the ocean water column at different depths. Using these measurements and a regional weather prediction model capable of simulating the isotopic composition, we find indications for an imprint of the atmospheric evaporation that is transferred into the mixed layer of the ocean over longer times. If our finding can be confirmed from additional measurements, such information can be used to constrain models with coupled atmosphere and ocean components, such as Earth System models.

1. Introduction

The Iceland and Greenland Seas are a region characterized by intense interaction between the atmosphere and the ocean (Renfrew et al., 2019). In particular during winter, cold and warm air masses meet over the partly ice-covered seas. Consequently, weather systems in the area during wintertime are characterized by strong air-sea interaction, and intense surface fluxes, both in terms of evaporation and precipitation (Papritz & Spengler, 2017; Renfrew et al., 2023; Woods & Caballero, 2016). Excursions of Arctic air over open waters, so-called marine cold-air outbreaks (mCAOs), create an atmospheric environment characterized by large fluxes of sensible and latent heat (Brümmer, 1999; Papritz, 2017). These fluxes contribute to the rapid build-up of relatively deep, convective boundary layers, with widespread mixed-phase clouds and ensuing precipitation (Abel et al., 2017). In contrast, warm and moist air masses intruding from the mid-latitudes in the North Atlantic storm track cause

Project administration: Harald Sodemann
Resources: Martin Werner
Software: Martin Werner
Validation: Ian A. Renfrew, Kjetil Våge
Visualization: Harald Sodemann, Emil Jeansson, Iris Thurnherr, Stefanie Semper, Kjetil Våge
Writing – original draft: Harald Sodemann, Emil Jeansson, Iris Thurnherr
Writing – review & editing: Harald Sodemann, Alexandra Touzeau, Emil Jeansson, Iris Thurnherr, Chris Barrell, Ian A. Renfrew, Stefanie Semper, Kjetil Våge

widespread positive temperature anomalies, cloud cover, and precipitation. When traveling further poleward, remaining water vapor can dramatically impact Arctic cloud cover on synoptic time scales (Pithan et al., 2018; Woods & Caballero, 2016; Woods et al., 2013).

The underlying ocean in the same region responds on both, short and substantially longer time scales to the short-lived atmospheric forcing from different weather systems (Renfrew et al., 2023). Warm and saline Atlantic Water enters the Norwegian Sea across the Greenland-Scotland Ridge and is progressively cooled and densified through heat loss to the atmosphere on its way northward (Hansen & Østerhus, 2000; Mauritzen, 1996). This transformed Atlantic Water is returned southward again at depth in the East Greenland Current (EGC) at the western boundary of the Nordic Seas (e.g., Håvik et al., 2017). Large oceanic heat fluxes near the ice edge, for example, during mCAOs (Renfrew & Moore, 1999), may densify the Atlantic-origin water in the EGC further (Moore et al., 2022; Våge et al., 2018) and also facilitate open-ocean convection in the central Greenland and Iceland Seas (Moore et al., 2015). Dense water formed in these interior basins is mainly transported toward gaps in the Greenland-Scotland Ridge in deep slope currents, such as the North Icelandic Jet (Figure 1b; Semper et al., 2019, 2020). The dense overflow waters from the EGC and the North Icelandic Jet cross the ridge in Denmark Strait and contribute to fill the deep North Atlantic (Tanhua et al., 2005; Våge et al., 2013). At the surface, the EGC carries cold, substantially fresher Polar Water south along the east coast of Greenland (Haine et al., 2015; Håvik et al., 2017).

The contribution of the many different components, and the different time scales of atmospheric and oceanic variability render the identification of changes in air-sea interaction and an assessment of net effects challenging. Consequently, the state of the high-latitude water cycle, with retreating sea ice (Parkinson & Cavalieri, 2008; Vihma, 2014), changes in precipitation amount and intensity, and increasing runoff from melting land ice (Böning et al., 2016) is associated with large uncertainty, also in light of climate warming. This uncertainty also extends to simulating the coupled water cycle in the region, both on weather prediction and climate time scales (Kähnert et al., 2021; Vihma et al., 2014).

Stable isotope analysis provides a tool to untangle some of these complex relationships. The stable water isotope composition is quantified in terms of $\delta^2H = ((R_{smp} - R_{std})/R_{std})$ and correspondingly the $\delta^{18}O$, as per-mil deviations of the isotope ratios R between rare and abundant water isotopes from Vienna Standard Mean Ocean Water (VSMOW) in precipitation, seawater, and water vapor. During phase changes, the heavy isotopes are less likely to transition to the vapor phase, as quantified by the equilibrium fractionation coefficients α of less than 1 (e.g., ${}^2\alpha_{v/l} = {}^2R_{vapor}/{}^2R_{liquid} = 0.8988$ at 0°C, Merlivat & Nief, 1967). The δ^2H and $\delta^{18}O$ values thus allow to distinguish the contribution of different processes and from different reservoirs to the total water budget (Craig & Gordon, 1965; Dansgaard, 1964). In the atmosphere, the water isotope composition reflects meteorological conditions at the water vapor origin, mixing, and during transport, mainly through the primary isotopes δ^2H and $\delta^{18}O$ (Aemisegger, 2018; Jouzel et al., 2013). Past ship-based vapor isotope measurements at various latitudes have related atmospheric stable water isotope variations to evaporation and mixing in the atmospheric boundary layer (Benetti et al., 2014, 2015; Gat et al., 2003).

The ocean water isotope composition generally varies within a much smaller range from VSMOW than the atmospheric isotope composition (LeGrande & Schmidt, 2006). Different water masses can carry substantially different signatures. For example, North Atlantic Water has been shown to reflect various degrees of evaporation, precipitation, and river runoff (Benetti et al., 2017). Riverine input in the Arctic Ocean is associated with signatures that are substantially more depleted in heavy isotopes than the North Atlantic (Bauch et al., 2011; Östlund & Hut, 1984). As this fresh Polar Water enters the Nordic Seas through Fram Strait with the EGC, the water isotope composition combined with salinity is an indicator for origin and mixing between different water masses in the region. However, available observational isotope data remain severely limited in the Nordic Seas, both regarding temporal and spatial coverage, and water depth.

In the atmosphere, the second order stable isotope parameter d-excess = $\delta^2H–8\cdot\delta^{18}O$ has often been used as a measure of the evaporation conditions of near-surface water vapor (Dansgaard, 1964; Merlivat & Jouzel, 1979; Pfahl & Sodemann, 2014). During both Arctic and Antarctic cruises, the d-excess in atmospheric vapor has been shown to co-vary with relative humidity, SST, and in particular relative humidity with respect to SST (Bonne et al., 2019; Kurita, 2011; Thurnherr et al., 2020; Uemura et al., 2008). Duscha et al. (2022) showed the rapid variation in near-surface water vapor d-excess with changing evaporation regimes during the onset of an mCAO in the Nordic Seas. Thurnherr et al. (2021) showed that warm-air and cold-air advection events carried distinct

21698996, 2024, 19, Downloaded from https://agupubs.onlinelibrary.wiley.com/doi/10.1029/2024JD041138, Wiley Online Library on [05/10/2024]. See the Terms and Conditions (https://onlinelibrary.wiley.com/terms-and-conditions) on Wiley Online Library for rules of use; OA articles are governed by the applicable Creative Commons License

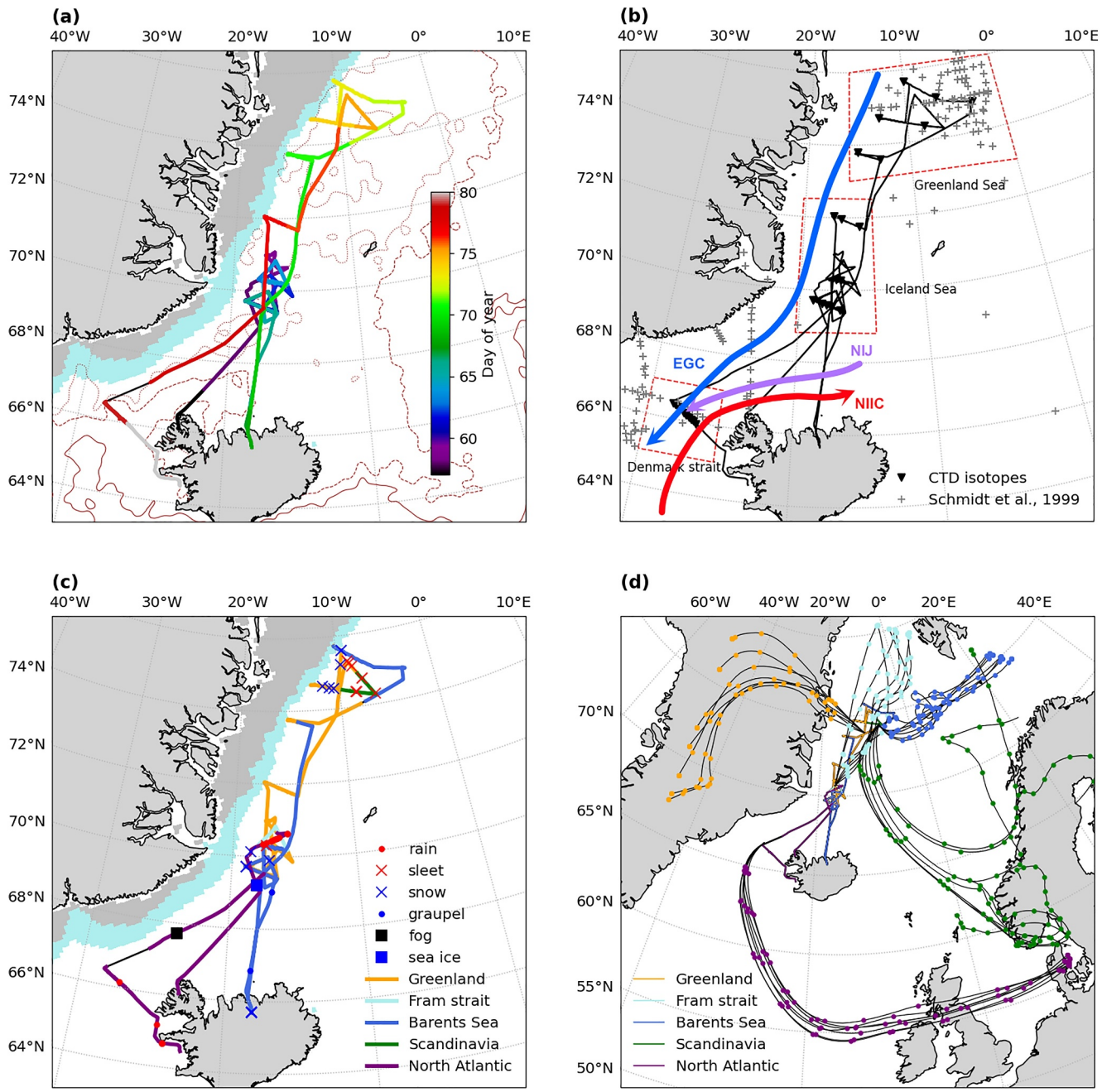

Figure 1. Ship track of NRV Alliance with water isotope measurements during leg 2 of the IGP cruise. (a) Time of ambient vapor isotope measurements (day of the year 2018, color), (b) sampling locations for seawater isotope measurements from CTD stations (black markers). Gray crosses indicate CTD stations retrieved from the database of Schmidt et al. (1999). Boxes denote groups of CTD stations. Arrows denote ocean currents, EGC = East Greenland Current (blue); NIJ = North Icelandic Jet (purple); NIIC = North Icelandic Irminger Current (red). (c) Locations of precipitation samples (markers) and classification of cruise track according to air mass transport (color). (d) Examples for air mass backward trajectories along different segments of Leg 2 of the IGP cruise. Brown contours in (a) show SST (C3S, 2019) with contours 0, 3, and 6°C, and shading in (a) and (c) shows sea ice edge data (Aaboe et al., 2023) with >70% (gray) and between 30% and 70% ice concentration (blue).

isotopic signatures in water vapor isotopes during the Antarctic Circumpolar Expedition cruise around Antarctica. Thereby, cold-air advection had a positive d-excess indicative of intense evaporation, while warm-air advection was associated with a negative d-excess as a result of condensation flux of vapor from the supersaturated atmosphere to the colder ocean. However, the corresponding imprint of the d-excess on oceanic waters has rarely been investigated. While continuous vapor isotope measurements have been made for several years onboard the R/V Polarstern including passages through the Nordic Seas on several occasions (Bonne et al., 2019), few studies

21698996, 2024, 19, Downloaded from https://agupubs.onlinelibrary.wiley.com/doi/10.1029/2024JD041138, Wiley Online Library on [05/10/2024]. See the Terms and Conditions (https://onlinelibrary.wiley.com/terms-and-conditions) on Wiley Online Library for rules of use; OA articles are governed by the applicable Creative Commons License

exist so far that conduct an isotopic survey in terms of main isotopes and the d-excess across the ocean-atmosphere system (Benetti et al., 2017), and none that specifically target the Iceland and Greenland Seas during winter.

Here we present an analysis of the ocean atmosphere coupling from a seaborne survey of the stable isotope composition in the water cycle across the ocean-atmosphere system in the Iceland and Greenland Seas during the Iceland-Greenland Seas project (IGP) cruise, which took place during the Year of Polar Prediction (YOPP) Special Observing Period (SOP) 1 in March 2018 (Renfrew et al., 2019). During the cruise, stable isotope measurements of water vapor, precipitation, and seawater were conducted alongside meteorological, hydrographic, and hydro-chemical measurements in an area that had not been covered previously by such combined sampling during winter. In this study, we investigate three key questions: (a) what is the state of the coupled atmosphere-ocean system in terms of stable water isotopes in the Iceland and Greenland Seas during winter? (b) How large is the variability in vapor and precipitation isotopes with different weather systems? (c) Can atmospheric variability in the form of evaporation and precipitation create an imprint on the mixed-layer isotope composition of the ocean? From our analysis, we document consistent signals emerging in relation to weather situations and the ocean currents in the area in terms of atmospheric vapor, precipitation, and seawater. Placed in the context of isotope-enabled regional model simulations, we also establish a baseline for comparison to airborne and land-based measurements of the water vapor isotope composition during IGP, that will be presented in forthcoming companion publications.

2. Data and Methods

This section provides a brief overview of the study area and campaign period for the ship-based water isotope measurements during the IGP, including the measurement platform, instrument installation, data processing, and numerical modeling in support of the data interpretation.

2.1. Campaign Period and Measurement Platform

The IGP campaign was a comprehensive international field campaign focused on atmosphere-ocean coupling and processes in the Iceland and Greenland Seas (Renfrew et al., 2019). Taking place during the Year of Polar Prediction Special Observations Period 1, the research cruise lasted from 6 February to 22 March 2018 and was separated in two legs. During Leg 2 of the IGP cruise, lasting from 26 February to 22 March 2018, water isotope instrumentation was installed on board NRV Alliance as part of the SNOWPACE research project. Precipitation samples were collected on the ship for stable isotope analysis. Furthermore, seawater samples from various stations and depths were obtained from CTD (conductivity, temperature, depth) casts. The research vessel also carried an extensive suite of instrumentation for atmospheric, hydrographic, and hydro-chemical measurements (Renfrew et al., 2019). Additional water vapor isotope measurements were performed in parallel with the Alliance cruise from the Twin Otter aircraft of the British Antarctic Survey operating out of Akureyri, Iceland, at a station in the harbor of Húsavik in northern Iceland, and at several locations in southern Norway, which will be published elsewhere.

During Leg 2 of the IGP cruise, the NRV Alliance departed from Ísafjörður in northwest Iceland on 26 February 2018 (DOY 57), then spent time east of Scoresbysund (Figure 1a, purple and blue colors). In this region, both liquid and solid precipitation samples were taken (Figure 1c, red and blue crosses, Table S1 in Supporting Information S1), as well as a CTD transect with water isotope sampling (Figure 1b, black markers, Table S2 in Supporting Information S1). Around DOY 70, the ship went to Akureyri, and after about 2 days in the harbor, it advanced into the Greenland Sea, thereby performing several west-east oriented transects toward the Marginal Ice Zone and the EGC (Figure 1b, blue arrow), reaching its northernmost location at 75.74°N on day 73 (Figure 1a, yellow color). Thereafter, the NRV Alliance progressively made its way toward Iceland, including a detailed CTD cross-section with 10 stations in Denmark Strait along the Greenland-Scotland Ridge near 66°N (Figure 1b, black markers, red boxes). At Denmark Strait, there are also influences from the dense water outflow in the North Icelandic Jet (NIJ, Figure 1b, purple arrow), and the Atlantic Water inflow in the North Icelandic Irminger Current (NIIC, Figure 1b, red arrow). A detailed analysis of the hydrography from the ocean profiles is found in Huang et al. (2021) and Renfrew et al. (2023). The ship returned to Reykjavik on 22 March 2018 (DOY 81).

21698996, 2024, 19, Downloaded from https://agupubs.onlinelibrary.wiley.com/doi/10.1029/2024JD041138, Wiley Online Library on [05/10/2024]. See the Terms and Conditions (https://onlinelibrary.wiley.com/terms-and-conditions) on Wiley Online Library for rules of use; OA articles are governed by the applicable Creative Commons License

2.2. Water Vapor Isotope Measurements

Water vapor and water vapor isotopic composition measurements were performed continuously during Leg 2 with a cavity ring-down laser spectrometer (CRDS; L2140-i, serial number HKDS2038, Picarro Inc., USA). The instrument was placed inside a heated measurement container on the boat deck of the NVR Alliance. The analyzer was run in air mode with a flow of 35 sccm through the cavity, and a 0.8 Hz data acquisition rate. The ambient air inlet was mounted at 4 m above the boat deck on a ladder leading to the radar antennas (Duscha et al., 2022; Figure 1). A downward-facing metal can with a diameter of 15 cm and height of 15 cm shielded the inlet from precipitation and sea spray. The uppermost 1.5 m of the inlet were a 3/8" stainless-steel tubing coated with sulfinert (SilcoTek, USA), integrated with self-regulating heat trace at 50°C and insulation (Thermon Inc. USA). This was followed by 2.5 m of 1/4" stainless steel tubing, also heated to 50°C, and wrapped with PE foam tape, which was then connected to a manifold pump (KNF 622N, KNF, Germany) that flushed the inlet at a flow rate of 5–10 standard liters per minute. The CRDS was connected with a T-piece to the inlet line inside the container, using 0.7 m of 1/8" stainless-steel tubing, protected by a check valve (Swagelok Inc, USA). Response tests on the inlet line with dry air indicated a response time of about 30 s for mixing ratio, and <120 s for both isotopes at a mixing ratio difference of 8,000 ppmv.

2.3. Water Vapor Isotope Data Processing

A vaporizer (A0211, Picarro Inc., USA) was installed for calibration of the analyzer by manual liquid injections. To this end, three secondary laboratory standards in use at the University of Iceland, Reykjavik (BERM, δ^2H of 6.26 ± 0.6, δ^{18}O of 0.52 ± 0.05; GV, δ^2H of −57.72 ± 0.6, δ^{18}O of −8.54 ± 0.05; NEEM, δ^2H of −257.11 ± 0.6, δ^{18}O of −33.52 ± 0.05), were injected daily into the vaporizer with a syringe, typically 8 times each, with approximate mixing ratios of 20,000 ppmv. Further data processing of the water vapor isotope measurements then follows the calibration routines in use at FARLAB (Facility for advanced isotopic research and monitoring of weather, climate and biogeochemical cycling), University of Bergen, Norway. Thereby, calibration periods are identified from the valve mask and removed with a 10 min time buffer before and after the injections. Next, raw isotope measurements are corrected for the mixing ratio-isotope ratio dependency using the method of Weng et al. (2020), as determined for this specific analyzer before and after the campaign period. The average correction was about −0.7‰ for δ^2H and −0.1‰ for δ^{18}O. Data were then normalized to VSMOW-SLAP scale according to recommendations by IAEA (2017), using the averages of all daily liquid injections of both laboratory standards (Figure S1 in Supporting Information S1). Drift of the measurement system in terms of d-excess was <0.5‰ over the campaign period. The uncertainty from calibration was quantified as 0.4‰ for δ^2H and 0.08‰ for δ^{18}O. The analytical uncertainty was estimated from the median standard deviation of 5-min averaging intervals, conditioned on mixing ratio in intervals of 1.0 g kg^{-1}. For the range of mixing ratios encountered during the cruise (~2,000–10,000 ppmv), the total propagated uncertainty was close to 1.0‰ for δ^2H and 0.2‰ for δ^{18}O, resulting in a total uncertainty of about 1.5‰ for the d-excess. Hourly and longer-time isotopic variations were typically one or two orders of magnitude larger than the respective combined uncertainty. Raw mixing ratios of $H_2{}^{16}O$ were corrected using a calibration established in the laboratory in comparison to a dew-point hygrometer. Quality flags were assigned to the data set, indicating if the instrument parameters exceeded operating specifications (80.000 ± 0.001°C for the cavity temperature, 45.0 ± 0.01°C for the wave-length monitor, and 50.0 ± 0.1 Torr for the cavity pressure).

The water vapor isotope data were then combined with meteorological data from two sets of meteorology sensors covering air temperature, wind speed, wind direction, relative humidity, and barometric pressure, and navigation data from NRV Alliance (Barrell & Renfrew, 2020; summary in Renfrew et al. (2021)). For the combination of data sets, all available variables were fused on a common 300 s time interval, thereby averaging higher-resolution continuous variables, and computing the median for higher-resolution flag variables. Before averaging, the vapor measurements were corrected for the time offset of the inlet line. The final, fused data file spans the period 22 February to 25 March 2018. The documented data set is available at the CEDA archive (Sodemann & Weng, 2022). Furthermore, as detailed in Renfrew et al. (2019), a total of 100 radiosondes were launched during the cruise to measure air temperature, winds and relative humidity above the ship (Brooks, 2019).

21698996, 2024, 19, Downloaded from https://agupubs.onlinelibrary.wiley.com/doi/10.1029/2024JD041138, Wiley Online Library on [05/10/2024]. See the Terms and Conditions (https://onlinelibrary.wiley.com/terms-and-conditions) on Wiley Online Library for rules of use; OA articles are governed by the applicable Creative Commons License

2.4. Precipitation and Seawater Sampling for Isotopic Analysis

In total, 60 precipitation samples have been collected for analysis of the water isotope composition (rain and snow), and one fog sample collected from a suspended mesh (Figure 1c, Table S1 in Supporting Information S1). Precipitation samples were mainly taken on the boat deck and occasionally on the surface of the aft deck. Daily precipitation (mostly rain) was sampled with a Hellmann-type accumulating rain sampler. More frequent rain sampling (typically hourly) was done with a simple manual collector for rain and snow (Weng et al., 2021). During high wind speeds, some lighter precipitation events were missed in the sampling. Snow samples were collected on different surfaces (balloon basket, life jacket box) on the aft deck into 58 ml sterile plastic bags (Whirl-Pak, USA), melted at room temperature and filtered before transferring an aliquot to 1.5 ml GC vials with rubber/PTFE septa (part #548-0907, VWR, USA). Samples with visible dirt were filtered with 25 mm Nylon filters with a 0.2 μm PTFE membrane (part #514-0066, VWR, USA) before being transferred to vials.

Out of the 189 CTD stations visited during the entire IGP cruise, 152 were sampled for a combination of tracers, including chlorofluorocarbon-12 (CFC-12), Sulfur hexafluoride (SF_6), dissolved oxygen (DO), apparent oxygen utilization (AOU) and occasionally nutrients (Renfrew et al., 2019). AOU is the difference between the saturation concentration and measured concentration of oxygen and gives an indication of how much oxygen that has been used since it was in contact with the atmosphere, and hence qualitatively indicates the age. In addition, at 29 selected CTD stations during Leg 2, a total of 272 seawater samples were collected for water isotope analysis (Figure 1b). These water samples were taken directly from the Niskin bottles after the samples for hydrochemistry had been taken (Table S2 in Supporting Information S1). The water samples for stable isotope analysis were taken at depths ranging from 7 to 500 m with an interval of 50 or 100 m. Samples were filled into 1.5 ml GC vials with rubber/PTFE without filtering. All water sample vials were sealed with Parafilm, stored upside down at room temperature during the cruise period, hereafter at 4°C, until being analyzed in the weeks after the cruise (Section 2.5, Tables S1 and S2 in Supporting Information S1).

2.5. Liquid Sample Analysis for Stable Water Isotope Composition and Seawater Chemistry

Precipitation and sea water samples were analyzed for their liquid water isotope composition in terms of $\delta^{18}O$ and $\delta^{2}H$ at FARLAB in the weeks after the campaign. An autosampler (A0325, Picarro Inc) transferred ca. 2 μl per injection into a high precision vaporizer (A0211, Picarro Inc, USA) heated to 110°C. After blending with dry N_2 (<5 ppm H_2O) the gas mixture was directed into the measurement cavity of a Cavity-Ring Down Spectrometer for about 7 min with a typical water concentration of 20,000 ppm. Memory effects were reduced by two times measuring a vapor mixture at a mixing ratio of 50,000 ppm, obtained from 2 injections of ca. 1.8 μl for 5 min at the beginning of each new sample vial. Thereafter, another 6 injections were measured for each sample. Data processing, including screening for outliers, memory correction, drift correction, and normalization, were done using the software tool FLIIMP V1.8.1 (Sodemann et al., 2023). For normalization to VSMOW-SLAP scale according to IAEA recommendations, the laboratory standards GSM1 ($\delta^{2}H$: -262.4 ± 0.6‰, $\delta^{18}O$: -32.98 ± 0.06‰) and EVAP ($\delta^{2}H$: 5.2 ± 0.6‰, $\delta^{18}O$: 5.09 ± 0.06‰) were used, and averaged over the beginning and end of each run. After memory correction using an exponential fit, the last 6 injections of each sample were averaged. Long-term reproducibility across different instruments is 0.05‰ for $\delta^{18}O$, 0.37‰ for $\delta^{2}H$, and 0.38‰ for d-excess, estimated from the $1-\sigma$ standard deviation for the repeated analysis of an internal laboratory standard over more than 1 year. One data point of station 110 (at depth 298 m) was an outlier that clearly showed evaporation effects and has been removed from the analysis. The final calibrated data are available in Sodemann and Weng (2022).

2.6. Isotope-Enabled Regional Model Simulations

Regional model simulations with water isotope composition were performed for the entire period of Leg 2 using the regional isotope-enabled model $COSMO_{iso}$ (Pfahl et al., 2012). To that end, the global reanalysis data set ERA5 (Hersbach et al., 2020) was first used for creating boundary conditions from the isotope-enabled general circulation model ECHAM5-wiso (Werner et al., 2011). Simulations with ECHAM5-wiso were run at a spectral resolution of T106L31, corresponding to approximately 125 km grid spacing in longitudinal and meridional direction. Sea-ice boundary conditions were taken from ERA5. The horizontal wind components in the $COSMO_{iso}$ domain were spectrally nudged to the boundary-condition winds above 850 hPa to keep the weather situation in the model domain close to the observed state, while allowing the model to develop its own representation of the lower-troposphere water cycle (Thurnherr et al., 2021). $COSMO_{iso}$ contains formulations for

21698996, 2024, 19, Downloaded from https://agupubs.onlinelibrary.wiley.com/doi/10.1029/2024JD041138, Wiley Online Library on [05/10/2024]. See the Terms and Conditions (https://onlinelibrary.wiley.com/terms-and-conditions) on Wiley Online Library for rules of use; OA articles are governed by the applicable Creative Commons License

isotope fractionation of δ^2H and δ^{18}O during phase changes, including the parameterization for moist deep convection. The surface ocean isotope composition was set uniformly to 0‰ for δ^2H and δ^{18}O. The model was configured with a 0.1° × 0.1° horizontal resolution, corresponding to about 10 km horizontal resolution in the domain, and 40 vertical levels. The lowest model level was on average at 10 m above the ocean. The simulation domain covered the Nordic Seas, including parts of Greenland, and southern Norway (Figure S2 in Supporting Information S1). The 8 grid points wide boundary zone of the simulation domain was removed from analysis. The simulation was run for the entire period of Leg 2, starting on 26 February 2018 at 00 UTC and ending at 12 UTC on 22 March 2018. For comparison with the measurements onboard NRV Alliance, time series were extracted from the model simulation at the grid point and lowest model level closest to the ship position, while interpolating in time between the hourly model output.

2.7. Backward Trajectory Calculations and Air Mass Classification

Air mass pathways during the IGP cruise were investigated using 4-day backward trajectories, calculated with Lagranto (Sprenger & Wernli, 2015; Wernli & Davies, 1997). To this end, hourly 3-dimensional winds from the $COSMO_{iso}$ simulation were used to calculate trajectories starting at the average location of the ship 30 min before and after the trajectory start time. In order to characterize the transport history of lower-tropospheric air, backward trajectories centered over the ship's mean position were computed starting at. 7 pressure heights (every 25 hPa between 1,000 and 850 hPa) at each hourly location of the vessel, approximately representing the boundary layer. The backward trajectories along the cruise track were manually classified into one of five categories, using the predominant transport path and air parcel locations 3 days back in time. The five pathways were: North Atlantic, Greenland, Fram Strait, Barents Sea, and Scandinavia, named according to the air parcel location 3 days before arriving at the research vessel (Figure 1c, shading). We chose here a simple manual classification of air mass pathways, rather than a diagnostic of water vapor source regions (e.g., Sodemann et al., 2008), as we deemed the potential interaction of air masses with the underlying surface during the last days of transport most relevant for the interpretation of the water isotope measurements on the NRV Alliance. Different flow paths for each of the five categories are exemplified in Figure 1d. Even though these cases were chosen as particularly clear examples, the categories proved to be distinct, except for the few hours when transitions between different air masses occurred. This air mass classification will be used below to interpret variations of isotope composition observed during the cruise.

2.8. Further Data and Tools for Isotopic Analysis

The d-excess over open water measures the extent of non-equilibrium conditions leading to kinetic fractionation. Earlier studies have shown that the d-excess co-varies with RH(SST), as a measure of the humidity gradient above the water surface (Merlivat & Jouzel, 1979; Uemura et al., 2008). Depending on the magnitude of the humidity gradient, and assuming non-negligible winds, a lower abundance of the slowly diffusing δ^{18}O in the vapor than expected from the δ^2H during equilibrium conditions results in a positive d-excess. In contrast, air that is supersaturated with respect to SST produces a condensation flux onto the ocean surface, whereby the faster diffusion of H^2HO than $H_2{}^{18}O$ can lead to low or negative d-excess values in the atmospheric vapor (Thurnherr et al., 2021). The variable RH(SST) is therefore an effective way to characterize the intensity of evaporation (flux per unit area) arising from the humidity imbalance between the water surface and atmosphere. RH(SST) was calculated as the ratio between the vapor pressure e, and the saturation vapor pressure e_{sat} at sea surface temperature (SST):

$$\mathrm{RH(SST)} = e/e_{sat}(\mathrm{SST}).$$

Airborne water vapor isotope measurements during IGP (Sodemann & Touzeau, 2022) were used to calculate end-members for the analysis of entrainment of free troposphere air into the boundary layer from selected flights. Three depleted end-members of atmospheric mixing analysis have been chosen based on four flights with the BAS Twin Otter aircraft with airborne water vapor isotope measurements that took place in the vicinity of the NRV Alliance on 4, 6, and 14 March 2018. The least depleted mixing end-member with an average δ^2H of −160.1‰ was obtained for the altitude range of 100–1,000 m and at latitudes north of 64°N, the most depleted end-member with an average δ^2H of −270.8‰ was obtained for the altitude range of above 2,500 m, and an

21698996, 2024, 19, Downloaded from https://agupubs.onlinelibrary.wiley.com/doi/10.1029/2024JD041138, Wiley Online Library on [05/10/2024]. See the Terms and Conditions (https://onlinelibrary.wiley.com/terms-and-conditions) on Wiley Online Library for rules of use; OA articles are governed by the applicable Creative Commons License

intermediate end-member at −220.0‰. As the specific humidity of the airborne measurements ranged between 0.8 and 1.5 g kg^{-1}, we chose q = 1.0 g kg^{-1} for the mixing line calculation.

2.9. Further Oceanographic Information

Measurements of the sea water isotope composition of oceanographic samples for the time period 1987–2010 have been extracted from the database of Schmidt et al. (1999). For the region from 34.98°E to 1.01°E and 65.03°N to 76.5°N, 1139 samples with a sampling depth of less than 800 m were obtained from the database.

Mixed-layer depth at the CTD stations was determined from a semi-automated multi-step procedure (Brakstad et al., 2019). In short, each temperature, salinity, and density profile was visually inspected. Two automated routines identified the base of the mixed layer, one based on a temperature difference criterion of $\Delta T = 0.2$ K and one based on the shallowest extremum in curvature of the temperature profile. When neither of the automated routines successfully identified the base of the mixed layer, the mixed-layer depth was determined manually by visually estimating the extent and the locations where the profile crossed outside a two-standard deviation envelope calculated over that depth range.

3. Observed State of the Atmosphere-Ocean System in Terms of Water Isotope Composition

Using the rare opportunity of a wintertime cruise, we now address our first research question and quantify the state of the coupled atmosphere-ocean system in terms of stable water isotopes in the Iceland and Greenland Seas during winter. The observations will also be used to assess the ability of the model simulation to represent the observed state in the same time period.

3.1. Synoptic Situation During the Cruise Period

Weather conditions during Leg 2 of the IGP campaign were in general dominated by a large, persistent anticyclone over Greenland that set up flow from the Barents Sea and Fram Strait, typical of mCAOs. The mCAO-dominated periods were characterized by shallow boundary-layer clouds with cloud streets, a form of organized convection characterized by parallel bands of cloud-free and cloudy air extending from the ice edge and mixed-phase clouds with cellular convection and intermittent precipitation (Duscha et al., 2022; Renfrew et al., 2023).

During the cruise, the ship sub-sampled the domain in time and space, and both ship motion and weather variation contributed jointly to variation in the measurement time series (Figure 2). Air temperature varied substantially during Leg 2 of the IGP cruise (Figure 2a, black line), but only partly in response to ship latitude (Figure 2a, green line). There were several marked episodes, lasting 1–2 days, where air temperatures reached below −8°C, such as on 04 March 2018, 12 March 2018, 15 March 2018, and 17 March 2018. These mCAO periods were related to the origin of the air from Greenland (Figure 2b, orange bar segments) and the Fram Strait (light blue bar segment) as primary sources of cold air. Events when the air masses had crossed over the Barents and Norwegian Seas (dark blue bar segments) were associated with more moderate temperatures, since these air masses had already experienced transformation over open waters. During the beginning and end of the cruise (26–28 February 2018, 19–22 March 2018), and an episode during 15–16 March, air temperatures close to 0°C prevailed, related to the intrusion of mid-latitude warm air from the southwest (purple) and southeast (green), as exemplified in Figure 1d. During 28 February 2018, a mid-latitude storm was encountered by the NRV Alliance, and liquid precipitation sampling was conducted north of 70°N (Figure 1c, red crosses). In the final days of the cruise (20–21 March 2018), the ship was again caught in a storm approaching from the south, with intense winds and liquid precipitation collected at latitudes between 64 and 66°N. These variations in weather conditions are partly reflected in histograms of atmospheric variables for Leg 2 (Figure S3 in Supporting Information S1). The complex temporal variation of air mass flow during the cruise is important for understanding the observed variations in the water vapor isotope composition.

3.2. Stable Isotope Composition of Near-Surface Water Vapor

The stable isotope composition of the water vapor at the height of the ship can be influenced by local and remote processes that impact phase changes and mixing state of the water vapor. With a median of −129.8‰, the δ^2H was well below −100‰ for most of the cruise period (Figure 2b), which is the theoretical δ^2H for vapor

21698996, 2024, 19, Downloaded from https://agupubs.onlinelibrary.wiley.com/doi/10.1029/2024JD041138, Wiley Online Library on [05/10/2024]. See the Terms and Conditions (https://onlinelibrary.wiley.com/terms-and-conditions) on Wiley Online Library for rules of use; OA articles are governed by the applicable Creative Commons License

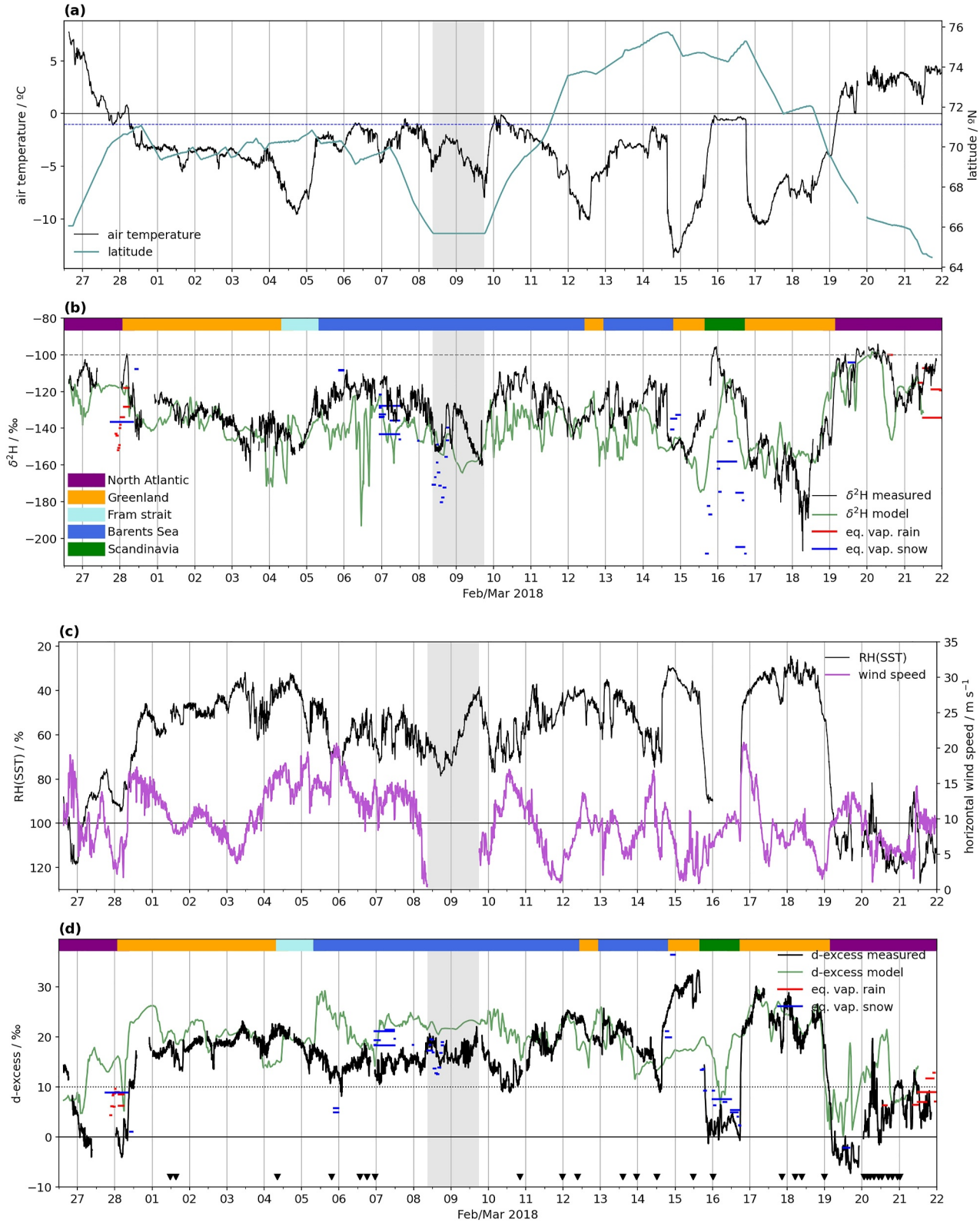

Figure 2.

21698996, 2024, 19, Downloaded from https://agupubs.onlinelibrary.wiley.com/doi/10.1029/2024JD041138, Wiley Online Library on [05/10/2024]. See the Terms and Conditions (https://onlinelibrary.wiley.com/terms-and-conditions) on Wiley Online Library for rules of use; OA articles are governed by the applicable Creative Commons License

emanating from the surface ocean during equilibrium conditions at these temperatures (Merlivat & Nief, 1967; Figure 2b, dashed gray line). This indicates that for most of the time air measured on the boat deck was a mixture between local surface evaporation and the advected free-tropospheric air entrained into the boundary layer (see Section 4.1). While temperature is in general an important factor for phase changes and thus isotope fractionation, the near-surface water vapor isotope composition does not very closely reflect variations in air temperature (Figure 2a), as expressed by a Pearson's correlation coefficient of r = 0.74 at 5 min time resolution. The time series for the $\delta^{18}O$ shows essentially the same characteristics (not shown), and thus discussion will focus here on δ^2H.

Short-term variation in δ^2H on a daily time scale can be influenced by the location of predominant weather systems, and by the geographical position, for example, in terms of proximity to sea ice and topography. Several episodes, where the δ^2H measurements had negative excursions show a change in predominant air transport. The most negative δ^2H was observed with −206.9‰ when very dry and depleted air that had passed over Greenland contributed to the mCAO during 18 March. Wind speeds briefly peaked at 15 m s^{-1} during the morning of that day (Figure 2c), enabling stronger vertical entrainment of low δ^2H air from the free-troposphere that had passed over Greenland into the marine boundary layer. Dewpoint temperatures of below −30°C dominated in an extensive layer up to at least 800 hPa over the ocean at this time (Figure S4a in Supporting Information S1, green line). Less negative excursions in δ^2H were observed for intrusions of warm air, such as on 26–28 February, 16 March, and from 19 to 22 March (Figure 2b). During these warm-air advection cases, the δ^2H was close to the theoretical equilibrium with the ocean water (Figure 2b, dashed line). This indicates that the air masses were close to saturation during these times, with latent heat fluxes close to zero or directed toward the sea surface. An example of the vertical atmospheric sounding shows an essentially saturated atmosphere between 800 hPa and the surface (Figure S4b in Supporting Information S1). Precipitation sampled on several occasions varied also substantially, and was generally not in equilibrium with surface water (Figure 2b, horizontal blue and red bars). The relation between vapor and precipitation isotopes is further explored in Section 3.4.

The model-simulated δ^2H interpolated to the ship's position (Figure 2b, green line) is generally more depleted in heavy isotopes than the observations (δ^2H bias: −8.7‰), but matches the observational data overall in terms day-to-day variability (root mean square error (RMSE): 16.9‰). The 1hr-averaged observations and model data are correlated with a slope of 0.653 and a correlation coefficient r = 0.58‰ $‰^{-1}$ (Figure S5a in Supporting Information S1). There are some periods where model results and observations disagree by several 10s of ‰. During 6 March 2018, a period with active convection cells and relatively strong winds, the model simulated large excursions of depleted air that are not reflected in the measurements. The period of Scandinavian air transport on 15–16 March is underpredicted in terms of onset and duration, and the brief episode with most depleted air during 18 March is missed by the model simulation. On sub-daily time scales, there is a noticeable degree of variability in the model simulation that arises from mesoscale structures in the simulation (see Section 4). While the sub-daily variations are of similar magnitude in model and observation, their timing and frequency differ, as expected for the moderate nudging that has been applied during the simulation.

3.3. Processes Shaping the Deuterium Excess in Atmospheric Vapor

While δ^2H characterizes an air mass in terms of transport, and mixing processes, the second-order parameter d-excess provides information about the deviation from equilibrium conditions during evaporation and condensation (Figure 2d, black line). With a mean of 15.1 ± 7.9‰, and a range between −7.3 and 33.3‰, the vapor d-excess was on average substantially further away from equilibrium conditions than the global average of about 10‰ (Figure 2d, dashed line). Such persistent non-equilibrium conditions are characteristic of the large humidity gradients leading to intense evaporation during mCAO events (Aemisegger & Papritz, 2018; Duscha et al., 2022). Overall d-excess maxima of above 25‰ were reached during two episodes when air descending from Greenland was encountered by the NRV Alliance close to the ice edge on 15 March (28‰), and from 17 to 19 March 2018

Figure 2. Time series of meteorological and isotope measurements during Leg 2 of the IGP cruise onboard NRV Alliance. (a) Air temperature (black, °C) and latitude of NRV Alliance (green, °N). (b) δ^2H (‰) from measurements (black line) and interpolated to the ship location from the nudged $COSMO_{iso}$ simulation (green line). Equilibrium vapor of precipitation sampled on the ship deck is shown by horizontal bars (red: liquid, blue: solid precipitation). Equilibrium vapor for evaporation of liquid water with a δ^2H of 0‰ at 0°C is shown by the gray dashed line. (c) Relative humidity calculated with respect to sea surface temperature (%, black line) and wind speed (m s^{-1}, purple line), (d) d-excess measured in ambient water vapor (‰, black line) and interpolated to ship position from nudged $COSMO_{iso}$ simulation (‰, green line). Red and blue lines in (b) denote d-excess in precipitation samples. Black triangles in (d) indicate CTD casts. The colored stripe on top indicates the air mass origin classification based on 4-day backward trajectories. The gray shaded region indicates the time period when NRV Alliance was in the harbor of Akureyri, Iceland.

21698996, 2024, 19, Downloaded from https://agupubs.onlinelibrary.wiley.com/doi/10.1029/2024JD041138, Wiley Online Library on [05/10/2024]. See the Terms and Conditions (https://onlinelibrary.wiley.com/terms-and-conditions) on Wiley Online Library for rules of use; OA articles are governed by the applicable Creative Commons License

(30‰). These were also the events where RH(SST) was at minimum. During the majority of the time, the RH (SST) was around 50%, with minimal values of below 30% reached on 18 March 2018 (Figure 2c).

There were only three events when the d-excess reached below 10‰, namely when the ship was in warm-air intrusions (Figure 2d, purple and green bar). In these saturated conditions, latent heat fluxes were close to zero or directed toward the sea surface. For all three cases, non-equilibrium processes quantified by the d-excess show that water vapor with high δ^2H condensed more easily onto the sea surface than water vapor with high δ^{18}O, leaving the remaining air with a low δ^2H relative to δ^{18}O, and thus a negative d-excess value as low as −7.3‰. The air was in these cases close to saturation, partly also above saturation with respect to the sea surface (RH (SST) > 100%, Figures 2c and 2d, purple and green segments). Major variations in RH(SST) are clearly reflected in the d-excess, resulting in a strong negative association with r = −0.86 between both variables for the 5-min data. Wind speeds were highly variable during Leg 2 (Figure 2c, purple line) and varied differently from RH (SST) and air temperature. Variations in wind speed do here not show an obvious relation to the d-excess (r = −0.06). The main role of the wind speeds in terms of isotope composition appears thus in mixing, aiding to replace saturated near-surface air with unsaturated air, and thus maintaining the evaporation process. With the sustained, high d-excess during the cruise period, the oceanic imprint of these evaporation conditions would be a negative d-excess in the surface water. This provides an important cue for investigating the oceanic imprint of atmospheric processes into the oceanic column in terms of stable water isotopes (see Section 5).

The simulated d-excess has a positive bias of 3.6‰ throughout the cruise, with a RMSE of 7.4‰. The correlation between model and observations has a slope of 0.786‰ ‰$^{-1}$ with r = 0.54 for the 1-hr averaged data (Figure S5b in Supporting Information S1). The model simulated several periods in close agreement with observations, such as the episode from 1 to 5 March 2018 with a d-excess close to 20‰, the period from 11–14 March 2018 to 17–19 March 2018. A large positive bias was simulated from 27 February to 1 March, possibly due to misplacement of the warm front. During a period characterized by changing air masses after 14 March 2018 12 UTC the model missed the measured increase in d-excess to values of above 30‰, and the observed low d-excess of around 2–3‰ on 16 March 2018. The deficiencies in the simulated d-excess thus appear to be partly related to the position of mesoscale features and air mass advection to the actual location of the ship. Overall, despite localized mismatches, the simulated d-excess reproduces the variations on a day-to-day time scale onboard NRV Alliance. In combination, this indicates that the processes related to phase changes due to the atmospheric state and air mass transport are represented reasonably well by the model. This finding is in agreement with Thurnherr et al. (2021) who reported a good representation of d-excess variability in near-surface water vapor with COSMO$_{iso}$ simulations over the Southern Ocean. Given similar levels of performance regarding δ^2H (Figure S5a in Supporting Information S1), we therefore consider the model simulation as a useful asset in interpreting the isotopic observations onboard NRV Alliance in a larger context.

3.4. Stable Isotope Composition of Precipitation

Precipitation is an important counterpart to the water vapor in our assessment of the isotopic state of the study region. Precipitation collected on deck on a daily or higher temporal resolution was categorized as rain, snow, sleet (melting snow), or graupel (Figures 1c and 3a). The liquid precipitation samples spanned a range of −3.2 to −67.5‰ in δ^2H, with a mean of −36.3‰ (Figures 3a, Table 1). The sleet samples spanned the broadest range, from −3.3 to −126.4‰, and a mean of −72.4‰, while the snow samples were spanning a range of −15.7 to −113.8‰, with a mean of −52.6‰. There were only two graupel samples (mean of −47.1‰). One fog sample, collected from a fine mesh during the WAI of 16 March 2018, had a δ^2H of −6.0‰. Light precipitation was difficult to collect and is underrepresented in our analysis. In terms of the d-excess of precipitation samples, the snow (mean of 17.3‰) and graupel samples (mean of 19.0‰) show the strongest imprint of non-equilibrium fractionation (Figure 3b, Table 1). The sleet and rain categories are substantially lower, even averaging below the global average of 10‰ with 5.4 and 8.1‰, respectively.

The differences between precipitation categories are further emphasized in a δ^2H versus d-excess diagram (Figure 3c). The fog sample clusters together with sea water and sea ice close to the origin of the diagram (Figure 3c, black and blue symbols). Graupel and most snow samples (Figure 3c, blue crosses and dots) have a high d-excess (∼18‰) and are moderately depleted (δ^2H ∼ −50‰), consistent with an expectation that these hydrometeors formed from vapor that has evaporated during mCAO conditions. In addition, strong kinetic effects will potentially have contributed to the positive d-excess signature in the snow (Jouzel & Merlivat, 1984; Markle

21698996, 2024, 19, Downloaded from https://agupubs.onlinelibrary.wiley.com/doi/10.1029/2024JD041138, Wiley Online Library on [05/10/2024]. See the Terms and Conditions (https://onlinelibrary.wiley.com/terms-and-conditions) on Wiley Online Library for rules of use; OA articles are governed by the applicable Creative Commons License

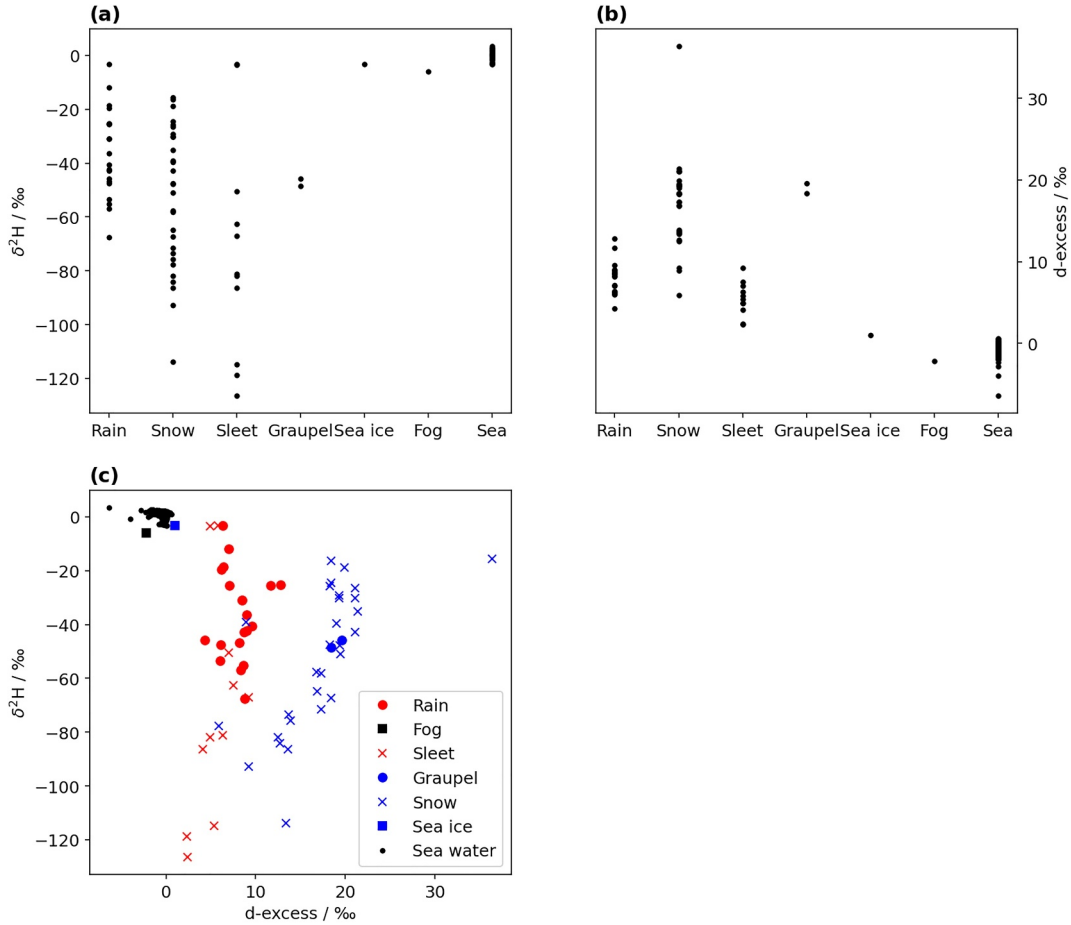

Figure 3. Water isotope composition of the 7 discrete sample categories collected during the IGP Leg 2 onboard NRV Alliance. (a) δ^2H (‰) for each sample category, (b) d-excess (‰) for each sample category, (c) δ^2H (‰) of each sample as a function of d-excess (‰).

& Steig, 2022). Some snow samples with a δ^2H < −60‰ tend toward a lower d-excess of 10‰, indicating that both longer-range transport and less intense evaporation, or (super-) saturated periods have been encountered. The rain and sleet samples (Figure 3c, red crosses and dots) group below 10‰ in d-excess. The most negative δ^2H is found in sleet samples, albeit with a d-excess that indicates substantial time in oversaturated conditions. Both aspects are indicative of a poleward intruding mid-latitude air mass that experienced prolonged, intense rainout and supersaturation. Precipitation from different weather systems can thus impose differing imprints on the isotope composition of the ocean mixed layer.

Table 1
Average, 1 − σ Standard Deviation, and Range of Stable Water Isotope Composition for Different Categories of Discrete Samples Taken During Leg 2 of the IGP Cruise

Type	Samples	δ^2H (‰)	Range	δ^{18}O (‰)	Range	d-excess (‰)	Range
Rain	20	−36.3 ± 16.1	[−67.5, −3.2]	−5.55 ± 2.03	[−9.54, −1.19]	8.1 ± 1.9	[4.3, 12.8]
Snow	29	−52.6 ± 25.7	[−113.8, −15.7]	−8.73 ± 2.81	[−15.89, −4.35]	17.3 ± 5.3	[5.9, 26.4]
Sleet	11	−72.4 ± 39.7	[−126.4, −3.3]	−9.73 ± 4.86	[−16.10, −1.04]	5.4 ± 2.0	[2.3, 9.2]
Graupel	2	−47.1 ± 1.4	[−48.4, −45.7]	−8.25 ± 0.09	[−8.35, −8.16]	19.0 ± 0.6	[18.4, 19.6]
Fog	1	−6.0	–	−0.48	–	−2.2	–
Sea ice	1	−3.3	–	−0.54	–	1.0	–
Seawater	272	1.5 ± 0.9	[−3.3, 3.5]	0.26 ± 0.15	[−0.41, 1.24]	−0.6 ± 0.6	[−6.4, 0.6]

21698996, 2024, 19, Downloaded from https://agupubs.onlinelibrary.wiley.com/doi/10.1029/2024JD041138, Wiley Online Library on [05/10/2024]. See the Terms and Conditions (https://onlinelibrary.wiley.com/terms-and-conditions) on Wiley Online Library for rules of use; OA articles are governed by the applicable Creative Commons License

3.5. Stable Isotope Composition of Sea Water

The water isotope composition in the Iceland and Greenland Seas can be influenced by local evaporation and precipitation, horizontal transport due to currents, and vertical mixing. As CTD casts during the IGP cruise have mainly been done in previously unsampled parts of the EGC within the Iceland Sea with regards to stable water isotopes (Figure 1b), they fill an important gap to disentangle various influences. The stable isotopes in seawater from the uppermost Niskin bottle (from depths ranging between 7 and 12 m) were enriched relative to VSMOW (δ^{18}O: 0.26‰, δ^{2}H: 1.5‰; Table 1). With regard to d-excess, seawater from all depths averages at −0.6‰, given the global average of 0‰ indicating an overall imprint of evaporation under non-equilibrium conditions on the sea water (Figure 3).

In the Greenland Sea (Figure 4a), our data points have an average δ^{18}O of 0.22‰ (dashed red line), which is still close to the typical inflow of Atlantic Water (0.3‰, gray dashed line) in the upper 800 m shown here. While there are only weak signs of freshwater near the surface that could be related to outflow from the transpolar drift (Charette et al., 2020), some freshening appears to have taken place in the upper 300 m. We place these measurements into the context of previous sporadic measurements of δ^{18}O over the years 1987–2010 acquired in the Greenland Sea to the north, and the Denmark Strait to the south. Many previous data had been taken further east in the Norwegian Sea (Figure 1b), and show an even closer correspondence to Atlantic isotope values throughout the profile (Figure 4a, gray crosses).

In the Iceland Sea, the profiles are different than in the Greenland Sea toward the surface (Figure 4b). The upper 200 m show considerable light freshwater signatures, whereas waters are still mostly close to Atlantic isotope conditions below, albeit with increased scatter. It is important to note that the differences in the column are not related to the east-west location of the sampling location (Figure S7a in Supporting Information S1), which is important because of the strong gradient in hydrographic conditions in this region. On average, the Iceland Sea profiles are slightly lighter at a δ^{18}O of 0.18‰. Although limited to a few samples only, the deepest water here has a tendency toward more positive δ^{18}O. In the d-excess profiles acquired from the Iceland Sea (Figure 4e), there is a substantially larger spread than further north in the Greenland Sea (Figure 4d). In particular, the d-excess reaches substantially further into negative values, which is consistent with a non-equilibrium evaporation signal mixed into the water column.

Finally, at the Denmark Strait transect, the southernmost water isotope CTD stations of the IGP cruise, the profiles are more depleted than further north, with an average δ^{18}O of 0.13‰. We identify two distinct limbs in the profile data (Figure 4c). A first limb is markedly light and fresh, with δ^{18}O of down to −0.5‰, indicative of Polar Surface Waters, while a second limb resembles more the (transformed) Atlantic Water observed in the Greenland Sea (Figure 4a). Interestingly, both limbs are also clearly present in the earlier measurements, and show a similar separation (Figure 4c, gray crosses). The clear separation of these two water masses in the upper 150 m shows that no mixing takes place at this depth. At the lowermost levels, there is again a tendency toward more enriched isotope values, as also supported by earlier measurements. The corresponding d-excess profile shows less negative d-excess at depth than in the Iceland Sea and resembles more the Greenland Sea profiles at depths greater than 300 m (Figure 4f). Also, the d-excess spans a wider range at Denmark Strait, with more negative values in the upper 300 m than in the Iceland Sea (Figure 4e). Since water isotope samples were taken across the entire Denmark Strait transect, we now further investigate the correspondence to other oceanic tracer variables.

West-to-east cross-sections of the Denmark Strait of potential temperature, Absolute Salinity, AOU, and δ^{18}O show different, yet partly corresponding patterns (Figure 5). The EGC is clearly visible in the western part of the section, as a 50 m deep layer of fresh and cold Polar Surface Water (Figure 5b, dark blue). There is a pronounced layer of Polar Surface Water over the Greenland shelf, and a weak warm anomaly below. The d-excess is mostly inhomogeneous in this region, with segments of d-excess above −0.5‰, and others that are more negative. There appear to be two kinds of dense water at depth, which is not so apparent in the salinity contour, but quite clear in terms of potential temperature, AOU and δ^{18}O. Within the uppermost 200–300 m, there are relatively small gradients in AOU, in line with a recent contact with the atmosphere (Figure 5d). Just below the Polar Surface Water and to the very west there could be recirculated Atlantic Water, with salinity above 35.1 g kg^{-1}, high potential temperature, and distinguished by δ^{18}O values of around 0.3‰.

In the eastern part, closest to Iceland, is Atlantic Water transported northward with the Irminger Current (Figure 1b, red arrow) into the Nordic Seas. This Atlantic water has high potential temperature (Figure 5a,

21698996, 2024, 19, Downloaded from https://agupubs.onlinelibrary.wiley.com/doi/10.1029/2024JD041138, Wiley Online Library on [05/10/2024]. See the Terms and Conditions (https://onlinelibrary.wiley.com/terms-and-conditions) on Wiley Online Library for rules of use; OA articles are governed by the applicable Creative Commons License

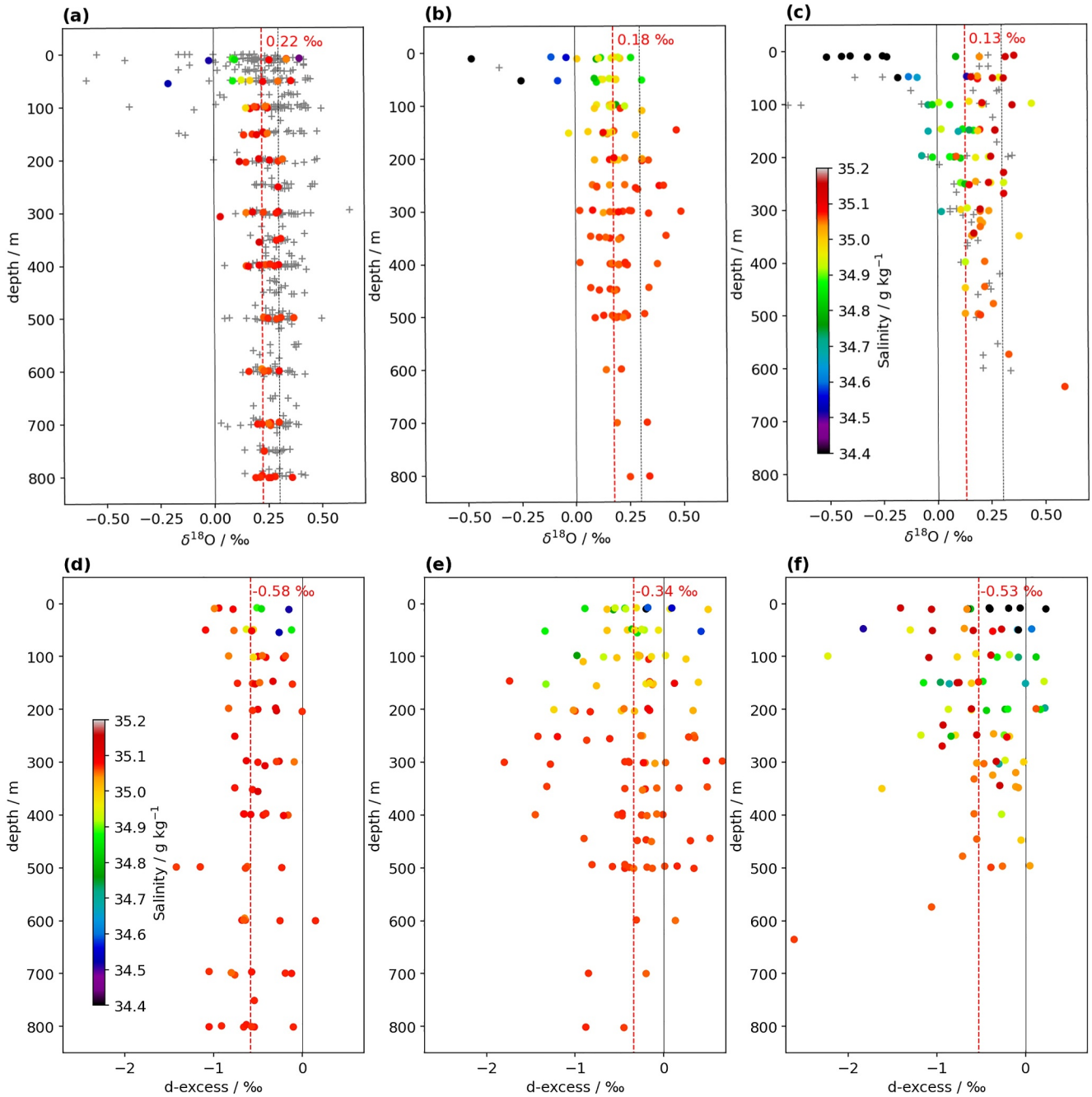

Figure 4. Seawater isotope composition of the upper 800 m, shaded by Absolute Salinity (g kg^{-1}) for (a) δ^{18}O in the Greenland Sea, (b) δ^{18}O in the Iceland Sea, (c) δ^{18}O in Denmark Strait, (d) d-excess in the Greenland Sea, (e) d-excess in Iceland Sea, and (f) d-excess in Denmark Strait. Gray dashed line in (a)–(c) indicates Atlantic Water δ^{18}O. Red dashed line is the mean of all IGP data in each region, with mean values given at the top. Gray crosses show CTD data retrieved from the database of Schmidt et al. (1999) for each region. Analytical uncertainty of the d-excess is 0.38‰.

$\theta > 5.5$°C), high salinity (Figure 5b, $S_A > 34.8$), homogeneous density (Figure 5c, $\sigma = 27.5$ kg m^{-3}), and is enriched in water isotopes (Figure 5e, δ^{18}O > 0.3‰). In the d-excess (Figure 5f) considerable noise is apparent throughout the cross section. Nonetheless, inflowing water of the NIIC on the Icelandic shelf has a d-excess of around −0.7‰, indicative of an evaporation imprint advected into the Iceland Sea.

The overflow water near the bottom (density $\sigma > 27.8$ kg m^{-3}) has a higher salinity and lower temperature than in the climatology of Mastropole et al. (2017), which is indicative of the presence of a so-called "bolus" in Denmark

21698996, 2024, 19, Downloaded from https://agupubs.onlinelibrary.wiley.com/doi/10.1029/2024JD041138, Wiley Online Library on [05/10/2024]. See the Terms and Conditions (https://onlinelibrary.wiley.com/terms-and-conditions) on Wiley Online Library for rules of use; OA articles are governed by the applicable Creative Commons License

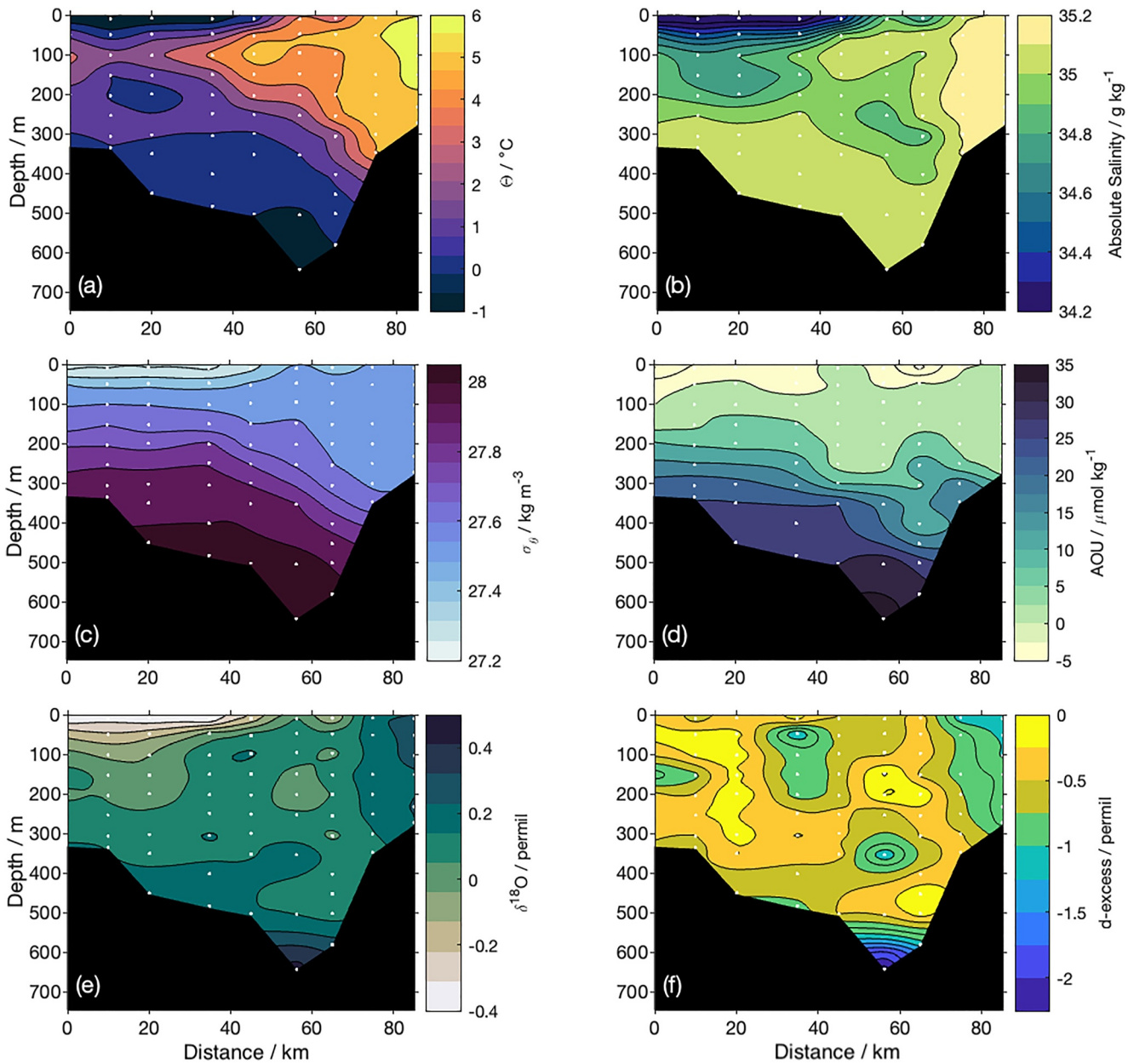

Figure 5. Vertical cross-sections from West to East (i.e., looking north) of different oceanographic variables across Denmark Strait. (a) Potential temperature (°C, shading), (b) Absolute Salinity (g kg^{-1}, shading), (c) potential density (kg m^{-3}, shading), (d) AOU (μmol kg^{-1}, shading), (e) δ^{18}O (‰, shading) and (f) d-excess (‰, shading). Iceland is to the right in the figure, and Greenland to the left. The white dots mark the sampled stations/depths.

Strait, a dense-water plume in the overflow water during the IGP cruise. At the bottom of the deepest CTD station, a δ^{18}O maximum of above 0.4‰ and an AOU maximum of above 30 μmol kg^{-1} was found. We also note that the δ^{18}O of this deepest, more aged sample is more positive than the Atlantic Water signature on the Iceland shelf. Albeit limited to two data points, there is also correspondence of this anomaly in potential temperature (Figure 5a) and with a d-excess of below −2.0‰. AOU indicates an old age for the deepest overflow water. Simple estimates show the influence of hydrothermal fluids on the ocean water is too small to play a measurable role in creating this anomaly (Jean-Baptiste et al., 1997).

Altogether, the question now becomes if and how the isotopic composition, and in particular the d-excess of inflowing sea water from the North Atlantic will be modified while residing in the Iceland and Greenland Seas.

21698996, 2024, 19, Downloaded from https://agupubs.onlinelibrary.wiley.com/doi/10.1029/2024JD041138, Wiley Online Library on [05/10/2024]. See the Terms and Conditions (https://onlinelibrary.wiley.com/terms-and-conditions) on Wiley Online Library for rules of use; OA articles are governed by the applicable Creative Commons License

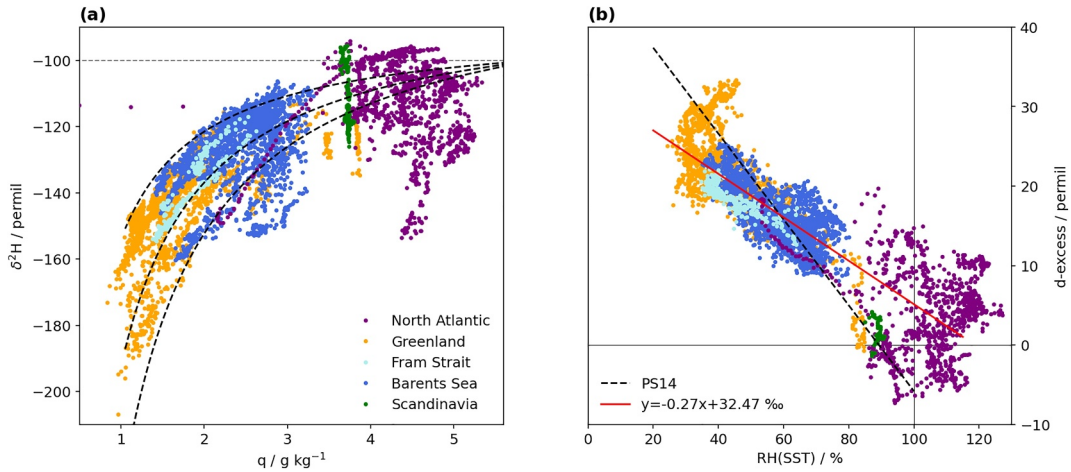

Figure 6. (a) Vapor mixing diagram for δ^2H during Leg 2 of the IGP cruise classified according to air origin (color). Equilibrium vapor with SST = 0°C and δ^2H = 0‰ is shown as a dashed gray line. Black dashed lines are obtained as mixing lines between equilibrium vapor from the sea surface and depleted end-members with −160.1‰, −220.0‰, and −270.8‰, respectively, at a specific humidity of 1.0 g kg^{-1}. (b) Correlation between d-excess and RH with respect to SST for the same data points. Overlaid are the linear relation by Pfahl and Sodemann (2014) (PS14, black dashed line) and a linear regression from this work (y = −0.27 × +32.47, red solid line).

Does the atmospheric variability related to mCAOs and WAIs cause a distinct and large enough imprint on the ocean? This will be investigated in the subsequent sections.

4. Quantifying Atmospheric Isotope Variability and Net Effects

The previous section demonstrated a wide range of variability in the atmospheric stable isotope composition during winter in the Iceland and Greenland Seas. Negative and positive d-excess signatures in vapor, positive d-excess in precipitation, and negative d-excess in the ocean column suggest that the atmospheric processes could imprint on the ocean system, contributing to an overall negative signal. We now investigate the net effect of different weather systems on the ocean using the isotope-enabled model simulation.

4.1. Isotopic Signatures of Mixing in the Atmospheric Boundary Layer

Rapid changes in weather systems imply that the water vapor measured in the atmospheric boundary layer by the ship is generally a mixture between local evaporation, vertical mixing, and atmospheric transport. Insight into the mixing state and end member contributions can be obtained from mixing diagrams of specific humidity and δ^2H (Figure 6a). The trajectory classification identifies that air with Greenland origin is located at the lower end of the mixing relation (yellow dots), whereas air from the Barents Sea is substantially less depleted (dark blue). Water vapor from Fram Strait takes intermediate positions (light blue). Several mixing lines are given in this mixing diagram (black dashed lines). The surface evaporation end-member with δ^2H = −100‰ is based on equilibrium fractionation of seawater (δ^2H = 0‰) evaporating at 0°C (Figure 6a, gray dashed line), whereas the other three end members are based on aircraft measurements during the campaign from different elevations (Section 2). These free-troposphere end-members indicate substantially depleted conditions, and thus cold condensation pathways for the air mixed into the boundary layer. The resulting three mixing lines clearly bracket the ship-based measurements for origins of Greenland, Fram Strait, and the Barents Sea. Accordingly, the most negative conditions coincide with cases where air masses passed over Greenland. Air masses with a very negative δ^2H signature are entrained from the free-troposphere air during roll cloud and cellular convection (Duscha et al., 2022; Renfrew et al., 2023).

The spread during Scandinavian (green dots) and North Atlantic origin air masses (purple dots) is not explained by the mixing lines. Instead, the variability is likely dominated by advective signals created from condensational rainout during transport. This separation is also underlined by the distinct gap in the data set at about 3.5 g kg^{-1}. Vertical signatures in the mixing diagram (large variation in δ^2H and relatively small variation in q) are likely due to non-local processes, such as rainout of the air mass during transport or a change of origin composition

21698996, 2024, 19, Downloaded from https://agupubs.onlinelibrary.wiley.com/doi/10.1029/2024JD041138, Wiley Online Library on [05/10/2024]. See the Terms and Conditions (https://onlinelibrary.wiley.com/terms-and-conditions) on Wiley Online Library for rules of use; OA articles are governed by the applicable Creative Commons License

(Noone, 2012), while the local humidity would be confined to saturation specific humidity by boundary-layer temperatures. The range of depletion in the purple and green data points would then reflect the condensation and rainout during the transport of these air masses. Similarly, the Barents Sea air masses (dark blue) could have been depleted in δ^2H while encountering small-scale convective showers that do not produce mixing lines.

A scatter plot of the measured d-excess versus RH(SST) shows the expected negative association, providing evidence of the importance of non-equilibrium fractionation under strongly unsaturated conditions (Figure 6b, yellow and light blue dots). Measurements classified with a North Atlantic pathway have a high RH(SST), and low or negative d-excess, indicating condensation flux onto the ocean surface (purple and green dots). A linear fit to all data points results in a relation with a slope of $-0.27‰\%^{-1}$ ($r = -0.86$). However, this relation is influenced by the supersaturated conditions during warm-air intrusion events (purple). A linear regression without those data points yields a slope of $-0.31‰\ \%^{-1}$ ($r = -0.79$). This value is close to the slope of $-0.4‰\ \%^{-1}$ found from measurements in the Southern Ocean (Thurnherr et al., 2020), but substantially lower than the slope of $0.54‰\%^{-1}$ obtained from a range of global data sets (Pfahl & Sodemann, 2014). There is also a strong negative association between the d-excess and air temperature ($r = -0.81$), which is however secondary to the physical process of non-equilibrium fractionation, quantified by RH(SST) (Merlivat & Jouzel, 1979). Note that there is only a weak negative association between the d-excess and the SST itself ($r = -0.13$), and with wind speed ($r = -0.06$) and wind direction ($r = -0.03$, not shown). Overall, this analysis confirms our interpretation of the d-excess as a signal of evaporation intensity, but also condensation intensity for this region for different weather patterns.

4.2. Contrasting Signals From mCAO and WAI Events

The variations in δ^2H and d-excess measured onboard NRV Alliance are always only a subsample of the temporal and spatial variability of these parameters in the entire Nordic Seas region. The fundamentally different atmospheric and isotopic state during mCAO and WAI periods are now quantified on a larger scale for two selected examples with the help of the regional model simulation.

First, we examine an mCAO event that dominated the study region on 4 March 2018. At 15 UTC, the NRV Alliance experienced generally northerly flow out of Fram Strait (Figure 7c, yellow lines). The vertically integrated water vapor (IWV) was on average 2–5 kg m^{-2}, but interspersed with bands of high IWV oriented perpendicular to the flow (Figure 7a). Moving toward the ship, these bands were associated with precipitation of up to 1.5 mm hr^{-1} from apparently partially organized convection (Figures 7a and 7c). The δ^2H at the lowest model level is mostly uniform, in contrast to the north-south gradient as in IWV, with anomalies that mirror structures in both IWV and precipitation (Figure 7e). Bands of pronounced gradients in δ^2H correspond to the precipitation field, with about $-160‰$ in some of the precipitation areas, followed by $-130‰$ or less at other locations. The spatial pattern in the d-excess field at this time in the simulation was dominated by a large-scale contrast between the d-excess near Greenland with values below 10‰ (Figure 7g, brown), and distinct patches of above 30‰ over the Norwegian Sea (purple). While some imprint of the precipitation bands is also apparent in the d-excess with values of around 15‰ (white), the d-excess predominantly carries a signal of the evaporation conditions associated with non-equilibrium fractionation due to large humidity gradients and high wind speeds at the ocean surface (Figure S6b in Supporting Information S1). The decrease in d-excess toward the southwest in this flow conditions reflects then the progressively weaker vertical humidity contrast above the ocean, leading to less negative or even positive latent heat fluxes (Figure S6a in Supporting Information S1), and thus weaker non-equilibrium fractionation.

Banded structures in the simulated δ^2H (Figure 7e) help to understand some of the sub-diurnal variability observed in the time series on the ship. We interpret the banded structure as a result of the preferential rainout of H^2HO over H_2O in precipitation areas, vertical mixing due to upward/downward motion, and below-cloud interaction of precipitation with the surrounding water vapor. As the NRV Alliance was overpassed by these bands of isotopic depletion, the day-to-day variability in δ^2H of up to 20‰ emerged that is visible in the ship measurements during 03–04 March 2018 (Figure 2b black line). Over the cold surface of Greenland, saturated conditions in the atmosphere cause preferential deposition of H^2HO relative to $H_2{}^{18}O$, resulting in a low and even negative d-excess. Filaments of this low d-excess air are sometimes advected toward the ship's position, before being overwritten by local evaporation (not shown).

As a contrasting example with WAI conditions, we depict the study domain on 16 March 2018. At 00 UTC, an intrusion of mid-latitude air had brought warm and moist air with an IWV of up to 15 kg m^{-2} into the Iceland Sea

21698996, 2024, 19, Downloaded from https://agupubs.onlinelibrary.wiley.com/doi/10.1029/2024JD041138, Wiley Online Library on [05/10/2024]. See the Terms and Conditions (https://onlinelibrary.wiley.com/terms-and-conditions) on Wiley Online Library for rules of use; OA articles are governed by the applicable Creative Commons License

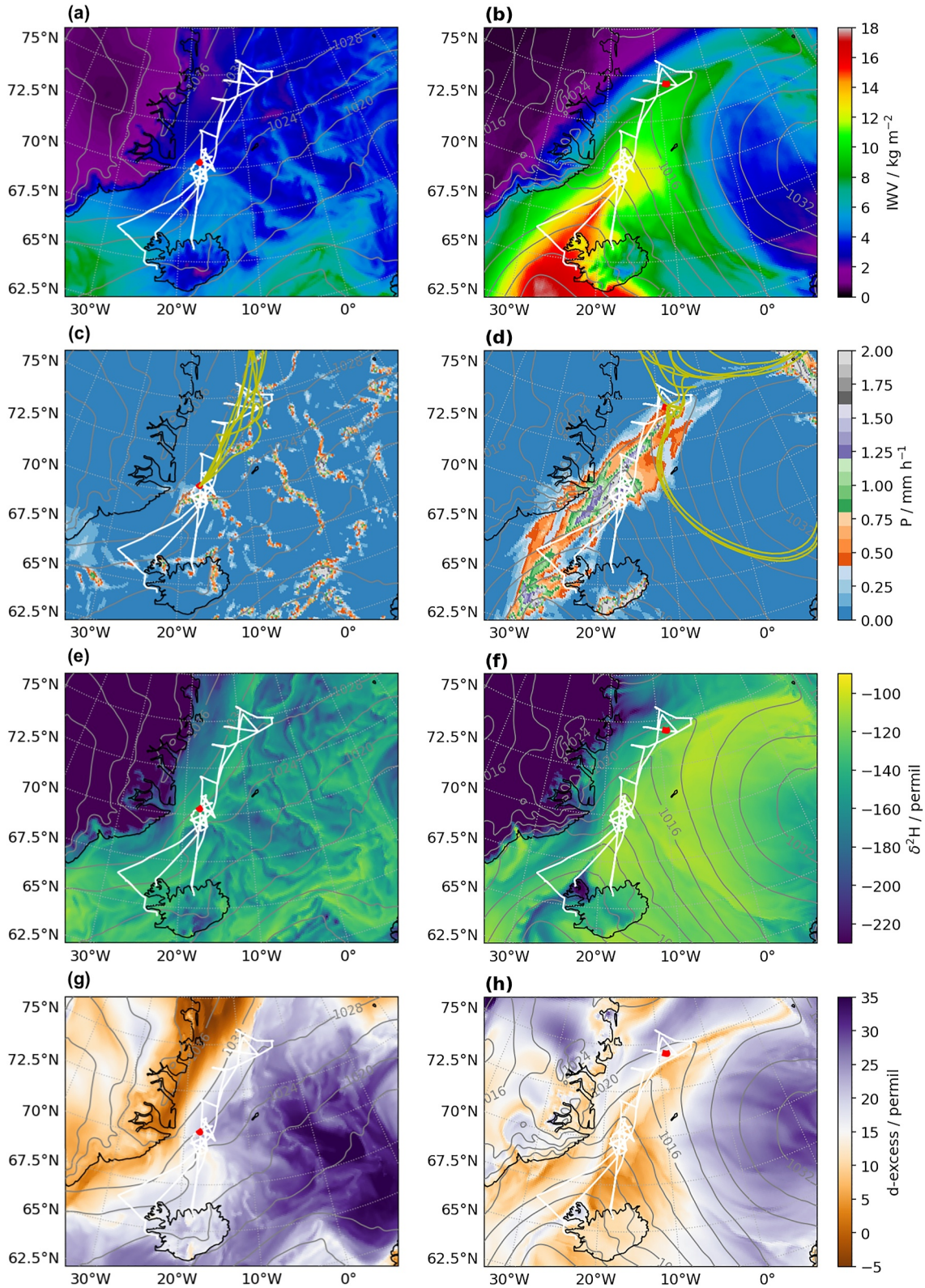

Figure 7. Atmospheric state in the Nordic Seas at 15 UTC on 4 March 2018 as simulated by the COSMO$_{iso}$ model. (a) Integrated water vapor (shading, kg m^{-2}), (c) total precipitation (shading, mm hr^{-1}) and 4-day backward trajectories started between 1,000 and 850 hPa at the ship position (yellow lines), (e) δ^2H in water vapor at the lowest model level (shading, ‰), and (g) d-excess in water vapor at lowest model level. The thin white line shows the cruise track during Leg 2 of the IGP cruise, and the red dot marks the ship's position at that time. Panels (b, d, f, h) show the same variables for 16 March 2018 at 00 UTC.

21698996, 2024, 19, Downloaded from https://agupubs.onlinelibrary.wiley.com/doi/10.1029/2024JD041138, Wiley Online Library on [05/10/2024]. See the Terms and Conditions (https://onlinelibrary.wiley.com/terms-and-conditions) on Wiley Online Library for rules of use; OA articles are governed by the applicable Creative Commons License

in the preceding days, reaching 9 kg m^{-2} to the ship's location at 74°N (Figure 7b). The corresponding sounding shows an almost saturated atmosphere up to 500 hPa (Figure S4b in Supporting Information S1). During its northward progression the WAI incorporated some air masses from southern Norway and from the Barents Sea (Figure 7d, yellow lines). Ample precipitation was shed by this air mass, exceeding 2 mm hr^{-1} in some areas of the Greenland Sea. The NRV Alliance was located right at the edge of the WAI air mass. The vapor δ^2H is simulated to be more uniformly distributed than during the mCAO (Figure 7f), with values of around −110‰. The remnant mCAO air along the Greenland coast is substantially more depleted. These sharp air mass gradients correspond to the pronounced variability observed in the δ^2H onboard the ship at that time, when the δ^2H decreased gradually from −90‰ on 16 March 2018 at 00 UTC until it sharply dropped to −160‰ at 22 UTC as the ship left the WAI (Figure 2b).

Pronounced east-west air mass differences were present in the d-excess on 16 March, with a sharp front line of d-excess less than 10‰ stretching from northwest Iceland across the Nordic Seas to Bear Island (Figure 7h). In the Norwegian Sea toward the east, cold air emanating from Scandinavia within the high pressure causes widespread evaporation in non-equilibrium conditions, leading to d-excess of above 20‰. The frontal band of low d-excess reflects the saturated mid-latitude air mass over relatively cold waters. Latent heat fluxes in the model are small or directed to the surface during this period in a broad sector from 68 to 72°N (Figure S6c in Supporting Information S1). Thereby, the preferential condensation of H^2HO compared to $H_2{}^{18}O$ creates a relative decrease in δ^2H in atmospheric water vapor, resulting in a low d-excess. The low d-excess measured onboard the NRV Alliance during 16 March corresponds well to the model simulation in this aspect, even if the magnitude and exact timing differ (Figure 2d).

The model simulation allows for a first-order assessment of the stable isotope composition in the atmospheric components in the study domain for both examples. Mass-weighted averaging of the isotope fluxes over the open ocean north of 67°N within the domain during the mCAO case on 4 March 2018 at 15 UTC provides a weighted average d-excess of 19.1‰ in vapor, 27.2‰ in rain, 21.1‰ in snow, and 37.2‰ in the evaporation, with a negative net E-P of −0.01 kg m^{-2}. This contrasts with the average signal of the WAI case on 16 March 2018 at 00 UTC, with 17.2‰ in vapor, 8.9‰ in rain, 14.5‰ in snow, and a positive net average E-P of 0.09 kg m^{-2}. While both of these examples are only instantaneous snapshots, the difference in d-excess between precipitation and evaporation can lead to a lowering of the oceanic d-excess, even if the net P-E is balanced or slightly positive.

5. Transfer of Atmospheric Variability Into the Ocean Water Column

Now we attempt to trace a potential isotopic imprint of net evaporation into the ocean mixed layer and the water column. In oceanography, it is most common to use $\delta^{18}O$ only as an isotopic tracer variable (e.g., Bauch et al., 2010). Here we will make use of both the δ^2H and $\delta^{18}O$, as well as the d-excess, enabling a connection to atmospheric measurements and net effects (Benetti et al., 2017).

5.1. Evaporation Imprints in Seawater Isotope Composition

Integration time scales in the ocean are substantially larger than those of atmospheric processes, leading to a much lower variability in sea water than in atmospheric measurements. The seawater δ^2H ranged between −3.3 and 3.5‰ during the campaign period, with an average of 1.5 ± 0.9‰ over all samples, while $\delta^{18}O$ ranged between −0.41 and 1.24‰, with an overall average of 0.26 ± 0.15‰ (Table 1). These resulting variation of 7‰ in δ^2H (1.65‰ for $\delta^{18}O$) is thus much smaller than the up to 123.2‰ (15.06‰ for $\delta^{18}O$) variation found between different precipitation samples, and the up to 112.7‰ (16.79‰ for $\delta^{18}O$) variation in water vapor (Table 2). Nonetheless, the long-term reproducibility of 0.38‰ for the d-excess from our analytical procedures (Section 2) enables interpretation of variation of small variations in the ocean isotope composition.

As the counterpart to the positive d-excess in atmospheric vapor (15.1 ± 7.9‰, Table 2), the on average negative d-excess in seawater samples (−0.6 ± 0.6‰, Table 1) corresponds to our expectation for the imprint of non-equilibrium fractionation at evaporation. We investigate the deviation from equilibrium using a δ^2H versus $\delta^{18}O$ scatter plot (Figure 8a). In equilibrium conditions, due to the eight times stronger fractionation for δ^2H, data points will line up along the black solid line with a slope of 8‰ $‰^{-1}$. In non-equilibrium conditions, $\delta^{18}O$ will increase faster and cause a lower slope, reflecting a negative d-excess. Water samples with a δ^2H of less than 1‰, mostly from areas with mixed layer depths of less than 20 m, appear to follow the equilibrium line (Figure 8a, orange, red and green dots). Their relatively light isotope composition points to contributions of water with Polar

21698996, 2024, 19, Downloaded from https://agupubs.onlinelibrary.wiley.com/doi/10.1029/2024JD041138, Wiley Online Library on [05/10/2024]. See the Terms and Conditions (https://onlinelibrary.wiley.com/terms-and-conditions) on Wiley Online Library for rules of use; OA articles are governed by the applicable Creative Commons License

Table 2
Average, 1 − σ Standard Deviation, and Range of Stable Water Isotope Composition for Different Air Masses Encountered During Leg 2 of the IGP Cruise

Type	δ^2H (‰)	Range	δ^{18}O (‰)	Range	d-excess (‰)	Range
All	−129.8 ± 16.6	[−206.9, −94.1]	−18.1 ± 2.87	[−28.44, −11.65]	15.1 ± 7.9	[−7.3, 33.3]
Greenland	−142.0 ± 14.2	[−206.9, −113.0]	−20.32 ± 2.20	[−28.44, −14.50]	20.5 ± 5.9	[−0.7, 33.3]
Barents Sea	−127.2 ± 10.9	[−160.4, −106.2]	−17.94 ± 1.64	[−22.60, −14.62]	16.2 ± 3.4	[8.1, 25.3]
Scandinavia	−111.1 ± 8.7	[−126.0, −95.5]	−14.19 ± 1.19	[−16.45, −12.07]	2.4 ± 1.5	[−1.3, 6.5]
North Atlantic	−113.4 ± 12.6	[−153.6, −94.1]	−14.72 ± 2.05	[−20.76, −11.65]	4.3 ± 5.7	[−7.3, 19.7]
Fram Strait	−138.9 ± 9.8	[−154.5, −117.1]	−19.63 ± 1.43	[−21.98, −16.54]	18.2 ± 1.9	[12.6, 22.1]

origin, which are known to possess a relatively light isotope composition due to the large runoff contributions from rivers in the Siberian and Canadian Arctic (Bauch et al., 1995). Most of these samples were taken within the ocean mixed layer determined from CTD measurements (denoted by circles in Figure 8), and are mostly located in the western basin, toward the EGC (Figure S7a in Supporting Information S1).

The seawater samples with mixed-layer depths larger than 20 m follow a flatter evaporation line with a slope of 4.4‰ ‰$^{-1}$, corresponding to a d-excess of about −2‰ (Figure 8a, blue dashed line). Evaporation lines with such a low slope are more commonly observed in Tropical Atlantic conditions and the Mediterranean than in North Atlantic water samples (Benetti et al., 2017). This could indicate that the evaporation signal of inflowing water from the North Atlantic is not only maintained, but further increased by more evaporation. The flatter slope being due to non-equilibrium evaporation, one could thus expect the relative humidity with respect to SST during evaporation in the Nordic Seas to be similarly low as in more southerly regions (Gat et al., 2003; Pfahl & Wernli, 2008). Consequently, we consider this slope as a possible sign of evaporation influence in the stable water isotope composition. In regions where ocean mixed layers are shallower than 20 m, other freshwater sources may overprint this evaporation influence. The few available data points from previous water isotope samples in the region confirm mainly the presence of a relatively depleted limb in this region, but also add a few data points in the cluster of evaporation-influenced samples observed here (Figure 8a, gray crosses). The implications of this potential evaporation imprint are further discussed in Section 5.2.

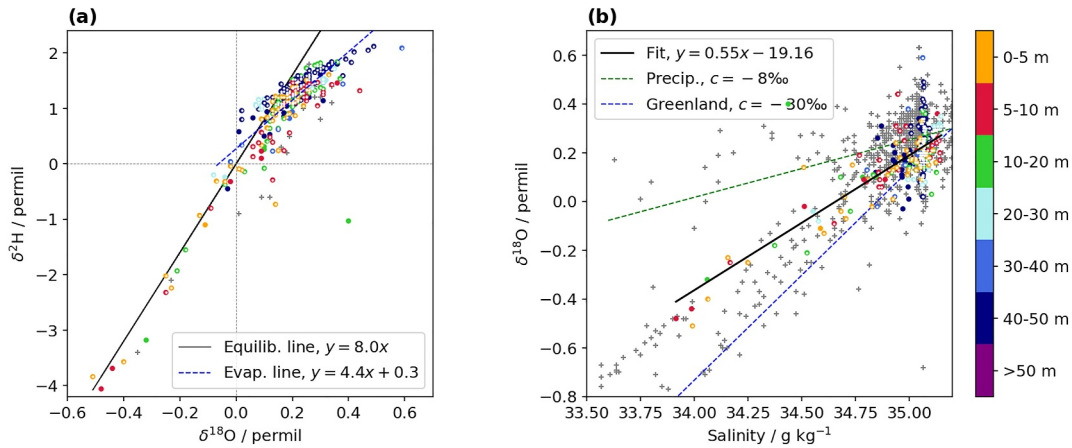

Figure 8. Seawater isotope composition of samples taken from CTD casts on NRV Alliance during Leg 2 of the IGP cruise. (a) Plot of δ^2H (‰) versus δ^{18}O (‰) with equilibrium line (y = 8.0x, solid black) and evaporation line (y = 4.4 × +0.3, dashed blue) obtained from a linear fit to the data points with a 10–40 m mixed layer depth. (b) Property plot of δ^{18}O (‰) versus Absolute Salinity (S_A, g kg^{-1}). Mixing lines between Atlantic end-member (δ^{18}O: 0.3‰, S_A: 35.2 g kg^{-1}) and local precipitation (−8.0‰, green dashed line) and Greenland meltwater (−32‰, blue dashed line) are shown for reference. Solid black line is a linear fit with an offset of δ^{18}O = −19.16‰ at SA = 0 g kg^{-1}. Color bar shows mixed layer depth categories. Colored circles indicate when samples were sampled within the ocean mixed layer depth, according to corresponding CTD measurements. Gray crosses are data points retrieved from Schmidt et al. (1999).

21698996, 2024, 19, Downloaded from https://agupubs.onlinelibrary.wiley.com/doi/10.1029/2024JD041138, Wiley Online Library on [05/10/2024]. See the Terms and Conditions (https://onlinelibrary.wiley.com/terms-and-conditions) on Wiley Online Library for rules of use; OA articles are governed by the applicable Creative Commons License

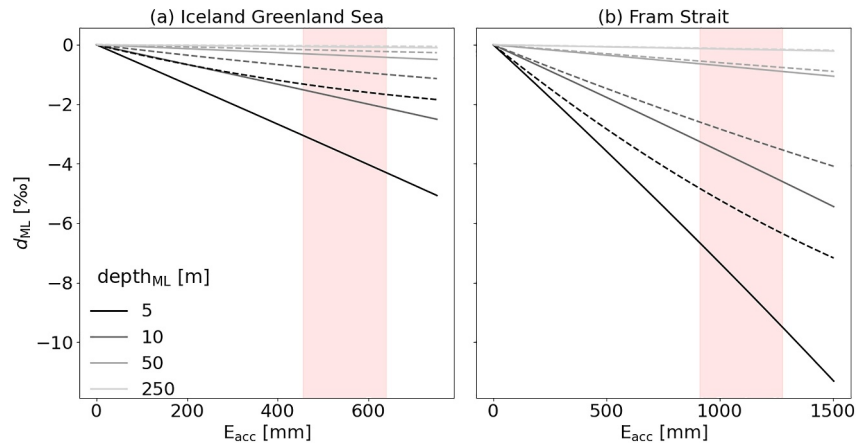

Figure 9. The evolution of d-excess in the ocean mixed layer (d_{ML}) during ocean evaporation using the Craig-Gordon model is shown as a function of accumulated ocean evaporation (E_{acc}) for (a) the Iceland and Greenland Seas and (b) Fram Strait. Different ocean mixed-layer depths are shown by the gray shades. Solid lines represent the simulations with q = 1.15 g kg^{-1}, in (a) 1.4 g kg^{-1} in (b), dashed lines for q = 2.25 g kg^{-1} in (a) and 3.0 g kg^{-1} in (b). The range of yearly accumulated evaporation is highlighted in red for (a) the Iceland and Greenland Seas and (b) Fram Strait.

Now we investigate the potential source of the freshwater in a δ^{18}O-salinity diagram (Figure 8b). Here, the surface water limb falls onto a mixing line with a freshwater end-member of about −19‰ in δ^{18}O (Figure 8b, solid line). Given the uncertainty of this extrapolation, the isotopically light end-member is in relatively close agreement with the −20 to −22‰ observed in Arctic river runoff (e.g., Östlund & Hut, 1984). The historical data (Figure 8b, gray crosses) show two other limbs that are not well captured by the IGP data. A first set of points falls onto a theoretical mixing line with an end-member of the IGP precipitation average of −8‰ in δ^{18}O (Figure 8b, green dashed line). A second set of the historical data points can be explained by a mixing line with a depleted end-member expected from Greenland ice sheet melt water (δ^{18}O of −30‰, blue dashed line in Figure 8b). As sea-ice formation and melt leads to salinity changes without strong isotope fractionation, some of the data points following a precipitation mixing line could also be explained by freezing and melting of sea ice, including brine rejection. While it is not possible to disentangle the different potential factors further here, we note that Arctic freshwater sources appear to dominate salinity gradients in the study region. Further analysis would be needed to clarify the impact of all possible factors.

5.2. Simulated Effect of Ocean Evaporation on Mixed-Layer Isotope Composition

We now attempt a simplified first-order estimate with regard to the potential impact of evaporation during non-equilibrium conditions on the ocean mixed layer. In a set of sensitivity experiments using the Craig-Gordon evaporation model (Craig & Gordon, 1965), we simulate air with a constant specific humidity and isotopic composition that moves over an ocean surface with constant SST. Preferential removal of the ^{2}H molecules due to their faster diffusion causes a positive d-excess in the vapor and a negative d-excess in the mixed layer. Thereby, we assume a constant bulk ocean mixed layer that does not exchange mass with the underlying ocean. To test different evaporation regimes, we use a mixed-layer temperature of 273.15 K (representative for the Iceland and Greenland Seas) and 277.15 K (representative for Fram Strait). Ocean evaporation does not affect the mixed-layer temperature, and the interface temperature is equal to the mixed-layer temperature. The model is set up to reflect typical evaporation rates during the winter season with an evaporation rate of about 3–4 mm day^{-1} (climatological average of ERA5 data in the Iceland and Greenland Seas). The air above the ocean is assumed to be continuously replaced by new air with the same properties. The isotopic composition of the ambient water vapor in a well-mixed, 1,000 m deep atmospheric boundary layer is taken as δ^2H = −100‰ and δ^{18}O = −12‰, leading to a d-excess in the water vapor of 4‰. The specific humidity (q) of the atmosphere is set to constant values in two sensitivity experiments representing RH(SST) of 20% and 60% in the Iceland and Greenland Sea, respectively.

According to our calculations, ocean evaporation causes a negative d-excess in the mixed layer that grows with increasing annual total evaporation E_{acc} (Figure 9a). Thereby, the magnitude of impact depends strongly on the ocean mixed-layer depths. For a mixed layer depth of 5 m, the d-excess decreases to −3‰ for the annual mean

21698996, 2024, 19, Downloaded from https://agupubs.onlinelibrary.wiley.com/doi/10.1029/2024JD041138, Wiley Online Library on [05/10/2024]. See the Terms and Conditions (https://onlinelibrary.wiley.com/terms-and-conditions) on Wiley Online Library for rules of use; OA articles are governed by the applicable Creative Commons License

evaporation in the Iceland and Greenland Seas (Figure 9a, red shading and black solid line). For an ocean mixed-layer depth larger than 50 m, the effect of ocean evaporation stays below −0.25‰ for the simulation time period (Figure 9a, solid light gray line). The decrease in d-excess in the ocean mixed layer also depends on the relative humidity and isotopic composition of the overlying air, the SST, and the ocean isotopic composition. Especially at higher SSTs, the RH_{SST} decreases, and thus non-equilibrium fractionation increases further. This is exemplified here for a setup that resembles the SST in Fram Strait (Figure 9b). With the larger annual mean evaporation in addition, the d-excess for a 10–50 m deep mixed layer can decrease between −0.5 and −4.0‰. Using the same setup, with the annual mean mixed-layer depth of 250 m gives a possible decrease in d-excess of about −0.1‰ from evaporation only. At more humid conditions the impact on the d-excess is reduced (Figure 9, dashed lines). In summary, calculations show that atmospheric conditions can potentially induce an imprint on the d-excess that is consistent with observations in terms of both sign and magnitude, and that would at least maintain an incoming negative d-excess signal. However, for a reliable estimation of the ocean evaporation effect on the ocean mixed layer, a dynamical simulation would be needed that includes the entire freshwater balance, as well as oceanic transport, mixing, and a time-variant mixed-layer depth.

6. Discussion

6.1. Traceability of Atmospheric Processes Into the Iceland and Greenland Seas Waters

During the IGP campaign, the average vapor composition indicated a prevalent control of boundary-layer water vapor by non-equilibrium fractionation processes (average d-excess 15.1‰). Such an evaporation regime is expected for mCAO conditions, characterized by large air-sea temperature and humidity contrasts and high wind speeds. Climatologically, mCAOs have been found to be responsible for 60%–80% of the wintertime sensible and latent heat loss from the ocean in the Greenland Sea, Fram Strait, and other nearby areas (Papritz & Spengler, 2017). Opposite heat fluxes during warm-air intrusions leading, for example, to dew deposition are an order of magnitude smaller than for mCAO conditions (Figure S6 in Supporting Information S1). Even though precipitation forms during mCAOs over ocean areas further downstream, the predominant mCAO imprint is thus a net evaporation signal with water vapor export, as also demonstrated in a case study with water vapor tracers for a large event (Papritz & Sodemann, 2018). Consequently, the non-equilibrium fractionation is expected to create a negative signal in the d-excess of the ocean mixed-layer on longer time scales (seasons to years), as a counterpart of the positive d-excess in the atmosphere.

With ocean mixed-layer depths encountered during IGP with a median of 57 m and ranging from 5 m to at most 322 m, the ocean is a much larger water reservoir than the boundary-layer vapor. It can therefore be questioned to what degree one can measure an evaporation signal in the ocean mixed-layer isotope composition given analytical uncertainties, and the intense wave regime and mixing during mCAOs. However, given that mCAOs are the prevailing wintertime weather system, a negative isotope signature can be hypothesized to build up over time within the mixed layer, and then be advected into the deeper ocean during convective events. Such a connection would be consistent with the wider range of negative d-excess values seen in the Iceland Sea samples (Figure 4e). Water entering from the North Atlantic carries an enriched evaporation imprint in the isotope composition of both δ^2H and $\delta^{18}O$, but with a d-excess closer to 0‰ (Benetti et al., 2017). The freshwater balance in the Nordic Seas during wintertime will potentially modify the d-excess with local evaporation during the time water spends in the system. Water samples from the Iceland Sea partly reach d-excess between −0.5 and −2.0‰ at depths of up to 250 m and below. It is tempting to interpret this isotopic signature as independent evidence of a mixed-layer depth exceeding 250 m in the Iceland Sea. This finding would be in good agreement with mixed-layer depths determined from high-resolution historical and recent hydrographic data (Våge et al., 2015, 2022). If confirmed, such a connection could be another important demonstration of the value of measuring both, $\delta^{18}O$ and δ^2H, to use the d-excess in oceanographic studies (Benetti et al., 2017). However, the general paucity of combined δ^2H and $\delta^{18}O$ from ocean water samples severely limits a definite observational proof of such isotopic connections. If isotopic information were available more broadly across the Nordic Seas, it could serve as independent observational constraint on the mass balance in the ocean and atmosphere in this region, providing valuable information for identifying ocean-atmosphere coupling, and for the development and testing of the water cycle representation in coupled ocean-atmosphere models (e.g., Brady et al., 2019).

21698996, 2024, 19, Downloaded from https://agupubs.onlinelibrary.wiley.com/doi/10.1029/2024JD041138, Wiley Online Library on [05/10/2024]. See the Terms and Conditions (https://onlinelibrary.wiley.com/terms-and-conditions) on Wiley Online Library for rules of use; OA articles are governed by the applicable Creative Commons License

6.2. Measurement and Model Results in the Context of Previous Studies

The western Nordic Seas in the winter season are characterized by large temperature contrasts, and substantially varying atmospheric conditions related to warm-air and cold-air advection. We now discuss differences and commonalities of the atmospheric water isotope composition measured here compared to previous observations taken in similar regions. Previous cruises covered mostly the summer, both in northern and southern high latitudes (Bonne et al., 2019; Kurita, 2011; Thurnherr et al., 2020; Uemura et al., 2008). The overall range of δ^2H and δ^{18}O during the IGP campaign was comparable to previous campaigns, except for periods when measurements were made within sea ice, or close to Antarctica (Bonne et al., 2019). While overall covering a similar range of variability, the maximum d-excess reported here of 33.1‰ was up to 10‰ larger than measured previously at similar latitudes, providing evidence of a large degree of non-equilibrium fractionation in evaporation during mCAOs and close to the ice edge during winter.

The isotopic variability with weather events resembled the findings of Thurnherr et al. (2021), who observed a decrease in d-excess during events of warm-air advection and an increase during cold-air advection in the Southern Ocean during the Antarctic Circumpolar Expedition cruise. Importantly, consistent with our study, their model simulations and observations show that the condensation flux in a supersaturated atmosphere induces pronounced gradients in the d-excess during warm-air advection events. Minimum d-excess here was as low as −7‰ during extended periods of predominant super-saturation of boundary layer vapor with respect to SST. Klein and Welker (2016) reported d-excess below 0‰ during a summertime cruise in the Bering Sea on several days within sea ice and during near-saturation with respect to air temperature. While being interpreted as an indication of sea-ice cover in their study, we find that the low d-excess is not necessarily connected to sea-ice cover, but a consequence of temperature differences between atmosphere and surface as a result of prevailing meteorological conditions. This notion is supported by the d-excess measurements of Bonne et al. (2019), which include several periods of negative d-excess reaching below −10‰, sometimes close to the sea ice edge, but not necessarily over sea ice. Negative or low d-excess values in atmospheric vapor or paleoclimate archives should thus not be considered exclusively as an indicator for sea-ice extent.

We also note a generally high level of consistency between the regional model simulation with COSMO$_{iso}$, driven by the global model ECHAM-WISO nudged to ERA5 reanalysis data, and the water vapor isotope measurements. That said, there are only few periods during the cruise when sea ice or snow-covered surfaces played a direct role for the isotope data, which have been observed to be the most challenging situations to be represented by models (Bonne et al., 2019). Instead, the water vapor isotope composition in the boundary layer was predominantly determined from mixing between ambient and advected water vapor and the local evaporation flux. Such overall consistency between model and observations in the absence of sea ice indicates that the representation and interplay of evaporation, condensation, and mixing in the model is, at least to first order, sufficient for our study.

7. Conclusions

Ship-borne measurements of the stable isotope composition of the coupled ocean-atmosphere system in the Iceland and Greenland Seas region during Leg 2 of the IGP cruise on NRV Alliance in February and March 2018 show a large degree of atmospheric variability. In line with previous studies, we find that cold-air outbreaks during the cruise are characterized by non-equilibrium fractionation that causes a distinct imprint in the evaporating vapor terms of δ^2H and δ^{18}O. In contrast to that, warm air intrusions from mid-latitudes lead to heat fluxes directed from the atmosphere to the surface, with different impacts on the isotopic composition. The dominant cause of variability of water vapor isotopes in the boundary layer appears to be the entrainment of depleted air from the free troposphere. Air masses passing over Greenland are thereby most depleted, followed by air masses arriving from Fram Strait, and lastly those that originate from the Barents Sea and pass over the Norwegian Sea. A more detailed analysis of water vapor sources and transport pathways for all water vapor isotope measurements during the IGP campaign using established moisture source diagnostics is currently in preparation.

Spatial extrapolation of the ship-based measurements with the isotope-enabled regional models COSMO$_{iso}$ support the plausibility of the atmospheric measurements by simulating both regional and mesoscale structures in the atmosphere that could explain variability on time scales from hours to several days. COSMO$_{iso}$ showed general agreement between model and observations in the vapor isotopes, except when the ship operated in a strong gradient close to the marginal ice zone. The performance quality of COSMO$_{iso}$ was probably facilitated by

21698996, 2024, 19, Downloaded from https://agupubs.onlinelibrary.wiley.com/doi/10.1029/2024JD041138, Wiley Online Library on [05/10/2024]. See the Terms and Conditions (https://onlinelibrary.wiley.com/terms-and-conditions) on Wiley Online Library for rules of use; OA articles are governed by the applicable Creative Commons License

the limited importance of sea ice and snow-covered surfaces for the isotopic composition of water vapor over the ocean during the NRV Alliance cruise.

The second-order parameter d-excess was found to be a key indicator variable to connect atmosphere-ocean interaction in terms of the stable isotope composition. With a measured average d-excess of 15.1‰ during the cruise, non-equilibrium conditions dominated, while warm-air intrusions lead to large contrasts of d-excess within a short distance. The average negative d-excess of −0.6‰ in sea water samples from the ocean mixed layer is consistent with a net export of high d-excess vapor out of the Nordic Seas region. Using a combination of the regional model simulation and a simple estimate of evaporation, we find the potential to explain the negative d-excess in the sea water as a buildup over seasonal to interannual time scales. A negative d-excess in the inflowing North Atlantic water could thus be maintained, or even strengthened. While the available evidence is overall consistent, further measurements of both δ^2H and δ^{18}O in ocean water are needed to more definitely establish such a connection between ocean and atmosphere in this region.

Values of the d-excess between −0.5 and −2.0‰ at depths of up to 250 m and below could provide independent evidence of a mixed-layer depth exceeding 250 m in the Iceland Sea from stable isotope measurements, in good agreement with other hydrographic data (Våge et al., 2015, 2022). Such a connection would be another example for the value of both stable isotope species, and the d-excess, in oceanographic studies (Benetti et al., 2017). Water isotopes also added information to the interpretation of AOC in the Denmark Strait transect, allowing to reiterate the suggestion by Mastropole et al. (2017) that additional transects with such multi-tracer approaches, for example, also further upstream across the EGC, could potentially provide valuable insight on factors that could contribute to changes in the EGC as the Arctic and in particular Greenland, respond to global warming.

Among the main implications of this work are that stable water isotopes reveal in-situ and time-integrated signatures from evaporation in both ocean and atmosphere. Stable water isotope measurements can thus enable both the detection of changes in the net imprint of atmospheric weather systems on the ocean, as well as enable the verification of the coupled mass balance of isotope-enabled models, both regional and global Earth System models. Comprehensive and coordinated sampling strategies over longer time will be needed to provide sufficiently robust constraints, in particular at the scale of global models.

Acknowledgments
This research has been supported by the Norges Forskningsråd (Grants 262710 and 245907). S.S. acknowledges support from the European Union's Horizon 2020 research and innovation programme under the Marie Skłodowska-Curie Grant Agreement 101022251. E.J. acknowledges support from the Research Council of Norway through the project VENTILATE (229791). FARLAB at University of Bergen is gratefully acknowledged for providing the vapor analyzer during the cruise. The IGP meteorological measurements were made possible by NERC Grant NE/N009754/1. We are grateful to Árný Erla Sveinbjörnsdóttir, Institute of Earth Sciences, University of Iceland, Reykjavik, for providing a vaporizer and calibration standards for the duration of the NRV Alliance cruise. We thank all people onboard the NRV Alliance who enabled the acquisition of the measurement data. Ulysses Ninnemann is acknowledged for helpful comments on an earlier version of this manuscript. The computations were performed on resources provided by Sigma2—the National Infrastructure for High-Performance Computing and Data Storage in Norway. This manuscript has partly been generated using Copernicus Climate Change Service information 2024. We thank three anonymous reviewers for their thorough and thoughtful comments which substantially improved the manuscript.

Data Availability Statement

The data presented in this paper can be obtained as follows: The documented stable isotope data set from the IGP cruise is available at the CEDA archive (url: https://dx.doi.org/10.5285/705abc2d9988444ba79e942f22219bc0, Sodemann & Weng, 2022), as well as radiosonde (url: https://catalogue.ceda.ac.uk/uuid/5acca11ececb4d8283b7e633370b6751/, Brooks, 2019) and surface-layer meteorological measurements (url: https://catalogue.ceda.ac.uk/uuid/b4ba8f11459c422d84d7293b9211ccf7/, Barrell & Renfrew, 2020). Airborne water vapor isotope data are also archived at CEDA (url: https://dx.doi.org/10.5285/7c8ce1c47da548a08146fa62158303c5, Sodemann & Touzeau, 2022). Sea-ice edge and sea surface temperature data are available from the Copernicus climate Change Service (https://doi.org/10.24381/cds.29c46d83, Aaboe et al., 2023; https://doi.org/10.24381/cds.cf608234, C3S, 2019). Historical sea water isotope data have been extracted from the database of Schmidt et al. (1999) (url: https://data.giss.nasa.gov/o18data/).

References

Aaboe, S., Down, E. J., Sørensen, A., Lavergne, T., & Eastwood, S. (2023). Sea-ice edge climate data record 1978-present, v3.0 [Dataset]. *Copernicus Climate Change Service (C3S) Climate Data Store (CDS)*. https://doi.org/10.24381/cds.29c46d83

Abel, S. J., Boutle, I. A., Waite, K., Fox, S., Brown, P. R. A., Cotton, R., et al. (2017). The role of precipitation in controlling the transition from stratocumulus to cumulus clouds in a Northern Hemisphere cold-air outbreak. *Journal of the Atmospheric Sciences*, *74*(7), 2293–2314. https://doi.org/10.1175/JAS-D-16-0362.1

Aemisegger, F. (2018). On the link between the North Atlantic storm track and precipitation deuterium excess in Reykjavik. *Atmospheric Science Letters*, *19*(12), e865. https://doi.org/10.1002/asl.865

Aemisegger, F., & Papritz, L. (2018). A climatology of strong large-scale ocean evaporation events. Part I: Identification, global distribution, and associated climate conditions. *Journal of Climate*, *31*(18), 7287–7312. https://doi.org/10.1175/JCLI-D-17-0591.1

Barrell, C., & Renfrew, I. (2020). Iceland Greenland seas Project (IGP): Surface layer meteorological measurements on board the NATO research vessel alliance [Dataset]. *Centre for Environmental Data Analysis*. Retrieved from https://catalogue.ceda.ac.uk/uuid/b4ba8f11459c422d84d7293b9211ccf7/

Bauch, D., Hölemann, J., Willmes, S., Gröger, M., Novikhin, A., Nikulina, A., et al. (2010). Changes in distribution of brine waters on the Laptev Sea shelf in 2007. *Journal of Geophysical Research*, *115*(C11), C11008. https://doi.org/10.1029/2010JC006249

21698996, 2024, 19, Downloaded from https://agupubs.onlinelibrary.wiley.com/doi/10.1029/2024JD041138, Wiley Online Library on [05/10/2024]. See the Terms and Conditions (https://onlinelibrary.wiley.com/terms-and-conditions) on Wiley Online Library for rules of use; OA articles are governed by the applicable Creative Commons License

Bauch, D., Rutgers van der Loeff, M., Andersen, N., Torres-Valdes, S., Bakker, K., & Abrahamsen, E. P. (2011). Origin of freshwater and polynya water in the Arctic Ocean halocline in summer 2007. *Progress in Oceanography*, *91*(4), 482–495. https://doi.org/10.1016/j.pocean.2011.07.017

Bauch, D., Schlosser, P., & Fairbanks, R. G. (1995). Freshwater balance and the sources of deep and bottom waters in the Arctic Ocean inferred from the distribution of $H_2{}^{18}O$. *Progress in Oceanography*, *35*(1), 53–80. https://doi.org/10.1016/0079-6611(95)00005-2

Benetti, M., Aloisi, G., Reverdin, G., Risi, C., & Sèze, G. (2015). Importance of boundary layer mixing for the isotopic composition of surface vapor over the subtropical North Atlantic Ocean. *Journal of Geophysical Research: Atmospheres*, *120*(6), 2190–2209. https://doi.org/10.1002/2014JD021947

Benetti, M., Reverdin, G., Aloisi, G., & Sveinbjörnsdottir, A. (2017). Stable isotopes in surface waters of the Atlantic Ocean: Indicators of ocean-atmosphere water fluxes and oceanic mixing processes. *Journal of Geophysical Research: Oceans*, *122*(6), 4723–4742. https://doi.org/10.1002/2017JC012712

Benetti, M., Reverdin, G., Pierre, C., Merlivat, L., Risi, C., Steen-Larsen, H. C., & Vimeux, F. (2014). Deuterium excess in marine water vapor: Dependency on relative humidity and surface wind speed during evaporation. *Journal of Geophysical Research: Atmospheres*, *119*(2), 584–593. https://doi.org/10.1002/2013JD020535

Böning, C., Behrens, E., Biastoch, A., Getzlaff, K., & Bamber, J. L. (2016). Emerging impact of Greenland meltwater on deepwater formation in the North Atlantic Ocean. *Nature Geoscience*, *9*(7), 523–527. https://doi.org/10.1038/ngeo2740

Bonne, J. L., Behrens, M., Meyer, H., Kipfstuhl, S., Rabe, B., Schönicke, L., et al. (2019). Resolving the controls of water vapor isotopes in the Atlantic sector. *Nature Communications*, *10*(1), 1632. https://doi.org/10.1038/s41467-019-09242-6

Brady, E., Stevenson, S., Bailey, D., Liu, Z., Noone, D., Nusbaumer, J., et al. (2019). The connected isotopic water cycle in the Community Earth System Model version 1. *Journal of Advances in Modeling Earth Systems*, *11*(8), 2547–2566. https://doi.org/10.1029/2019MS001663

Brakstad, A., Våge, K., Håvik, L., & Moore, G. W. K. (2019). Water mass transformation in the Greenland Sea during the period 1986–2016. *Journal of Physical Oceanography*, *49*(1), 121–140. https://doi.org/10.1175/JPO-D-17-0273.1

Brooks, B. J. (2019). Iceland Greenland seas Project (IGP): Upper air sounding: Profiles of temperature, pressure, humidity, wind speed and wind direction [Dataset]. *Centre for Environmental Data Analysis*. Retrieved from https://catalogue.ceda.ac.uk/uuid/5acca11ececb4d8283b7e633370b6751/

Brümmer, B. (1999). Roll and cell convection in wintertime arctic cold-air outbreaks. *Journal of the Atmospheric Sciences*, *56*(15), 2613–2636. https://doi.org/10.1175/1520-0469(1999)056<2613:racciw>2.0.co;2

Charette, M. A., Kipp, L. E., Jensen, L. T., Dabrowski, J. S., Whitmore, L. M., Fitzsimmons, J. N., et al. (2020). The Transpolar Drift as a source of riverine and shelf-derived trace elements to the central Arctic Ocean. *Journal of Geophysical Research: Oceans*, *125*(5), e2019JC015920. https://doi.org/10.1029/2019JC015920

Copernicus Climate Change Service (C3S). (2019). Sea surface temperature daily data from 1981 to present derived from satellite observations [Dataset]. *Copernicus Climate Change Service (C3S) Climate Data Store (CDS)*. https://doi.org/10.24381/cds.cf608234

Craig, H., & Gordon, L. I. (1965). Deuterium and oxygen-l 8 variations in the ocean and the marine atmosphere. In E. Tongiorgi (Ed.), *Stable isotopes in oceanographic studies and paleotemperatures* (pp. 9–130). Laboratorio di Geologia Nucleare.

Dansgaard, W. (1964). Stable isotopes in precipitation. *Tellus*, *16*(4), 436–468. https://doi.org/10.1111/j.2153-3490.1964.tb00181.x

Duscha, C., Barrell, C., Renfrew, I. A., Brooks, I. M., Sodemann, H., & Reuder, J. (2022). A ship-based characterization of coherent boundary-layer structures over the lifecycle of a marine cold-air outbreak. *Boundary-Layer Meteorology*, *183*(3), 355–380. https://doi.org/10.1007/s10546-022-00692-y

Gat, J. R., Klein, B., Kushnir, Y., Roether, W., Wernli, H., Yam, R., & Shemesh, A. (2003). Isotope composition of air moisture over the Mediterranean Sea: An index of air-sea interaction pattern. *Tellus B: Chemical and Physical Meteorology*, *55*(5), 953–965. https://doi.org/10.3402/tellusb.v55i5.16395

Haine, T. W. N., Curry, B., Gerdes, R., Hansen, E., Karcher, M., Lee, C., et al. (2015). Arctic freshwater export: Status, mechanisms, and prospects. *Global and Planetary Change*, *125*, 13–35. https://doi.org/10.1016/j.gloplacha.2014.11.013

Hansen, B., & Østerhus, S. (2000). North Atlantic—Nordic Seas exchanges. *Progress in Oceanography*, *45*(2), 109–208. https://doi.org/10.1016/S0079-6611(99)00052-X

Håvik, L., Pickart, R. S., Våge, K., Torres, D., Thurnherr, A. M., Beszczynska-Möller, A., et al. (2017). Evolution of the East Greenland Current from Fram Strait to Denmark Strait: Synoptic measurements from summer 2012. *Journal of Geophysical Research: Oceans*, *122*(3), 1974–1994. https://doi.org/10.1002/2016JC012228

Hersbach, H., Bell, B., Berrisford, P., Hirahara, S., Horányi, A., Muñoz-Sabater, J., et al. (2020). The ERA5 global reanalysis. *Quarterly Journal of the Royal Meteorological Society*, *146*(730), 1999–2049. https://doi.org/10.1002/qj.3803

Huang, J., Pickart, R. S., Bahr, F., McRaven, L. T., & Xu, F. (2021). Wintertime water mass transformation in the western Iceland and Greenland Seas. *Journal of Geophysical Research: Oceans*, *126*(8), 2020JC016893. https://doi.org/10.1029/2020jc016893

IAEA (INTERNATIONAL ATOMIC ENERGY AGENCY). (2017). *Reference sheet for VSMOW2 and SLAP2 international measurement standards* (p. 8). IAEA. Retrieved from https://nucleus.iaea.org/sites/AnalyticalReferenceMaterials/Shared%20Documents/ReferenceMaterials/StableIsotopes/VSMOW2/VSMOW2_SLAP2.pdf

Jean-Baptiste, P., Charlou, J. L., & Stievenard, M. (1997). Oxygen isotope study of mid-ocean ridge hydrothermal fluids: Implication for the oxygen-18 budget of the oceans. *Geochimica et Cosmochimica Acta*, *61*(13), 2669–2677. https://doi.org/10.1016/s0016-7037(97)00090-2

Jouzel, J., Delaygue, G., Landais, A., Masson-Delmotte, V., Risi, C., & Vimeux, F. (2013). Water isotopes as tools to document oceanic sources of precipitation. *Water Resources Research*, *49*(11), 7469–7486. https://doi.org/10.1002/2013WR013508

Jouzel, J., & Merlivat, L. (1984). Deuterium and oxygen 18 in precipitation, modeling of the isotopic effects during snow formation. *Journal of Geophysical Research*, *89*(D7), 11749–11757. https://doi.org/10.1029/jd089id07p11749

Kähnert, M., Sodemann, H., de Rooy, W. C., & Valkonen, T. M. (2021). On the utility of individual tendency output: Revealing interactions between parameterized processes during a marine cold air outbreak. *Weather and Forecasting*, *36*, 1985–2000. https://doi.org/10.1175/WAF-D-21-0014.1

Klein, E. S., & Welker, J. M. (2016). Influence of sea ice on ocean water vapor isotopes and Greenland ice core records. *Geophysical Research Letters*, *43*(24), 12475–12483. https://doi.org/10.1002/2016GL071748

Kurita, N. (2011). Origin of Arctic water vapor during the ice-growth season. *Geophysical Research Letters*, *38*(2), L02709. https://doi.org/10.1029/2010GL046064

LeGrande, A. N., & Schmidt, G. A. (2006). Global gridded data set of the oxygen isotopic composition in seawater. *Geophysical Research Letters*, *33*(12), L12604. https://doi.org/10.1029/2006GL026011

Markle, B. R., & Steig, E. J. (2022). Improving temperature reconstructions from ice-core water-isotope records. *Climate of the Past*, *18*(6), 1321–1368. https://doi.org/10.5194/cp-18-1321-2022

21698996, 2024, 19, Downloaded from https://agupubs.onlinelibrary.wiley.com/doi/10.1029/2024JD041138, Wiley Online Library on [05/10/2024]. See the Terms and Conditions (https://onlinelibrary.wiley.com/terms-and-conditions) on Wiley Online Library for rules of use; OA articles are governed by the applicable Creative Commons License

Mastropole, D., Pickart, R. S., Valdimarsson, H., Våge, K., Jochumsen, K., & Girton, J. (2017). On the hydrography of Denmark Strait. *Journal of Geophysical Research: Oceans*, *122*(1), 306–321. https://doi.org/10.1002/2016jc012007

Mauritzen, C. (1996). Production of dense overflow waters feeding the North Atlantic across the Greenland- Scotland Ridge. Part 1: Evidence for a revised circulation scheme. *Deep-Sea Research I*, *43*(6), 769–806. https://doi.org/10.1016/0967-0637(96)00037-4

Merlivat, L., & Jouzel, J. (1979). Global climatic interpretation of the deuterium-oxygen 18 relationship for precipitation. *Journal of Geophysical Research*, *84*(C8), 5029–5033. https://doi.org/10.1029/jc084ic08p05029

Merlivat, L., & Nief, G. (1967). Fractionnement isotopique lors des changements d'état solide-vapeur et liquide-vapeur de l'eau à des températures inférieures à 0°C. *Tellus*, *19*(1), 122–127. https://doi.org/10.1111/j.2153-3490.1967.tb01465.x

Moore, G. W. K., Våge, K., Renfrew, I. A., & Pickart, R. S. (2022). Sea-ice retreat suggests re-organization of water mass transformation in the Nordic and Barents Seas. *Nature Communications*, *13*(1), 67. https://doi.org/10.1038/s41467-021-27641-6

Moore, G. W. K., Våge, K., Pickart, R. S., & Renfrew, I. A. (2015). Decreasing intensity of open-ocean convection in the Greenland and Iceland Seas. *Nature Climate Change*, *5*, 877–882. https://doi.org/10.1038/nclimate2688

Noone, D. (2012). Pairing measurements of the water vapor isotope ratio with humidity to deduce atmospheric moistening and dehydration in the tropical midtroposphere. *Journal of Climate*, *25*(13), 4476–4494. https://doi.org/10.1175/JCLI-D-11-00582.1

Östlund, H. G., & Hut, G. (1984). Arctic Ocean water mass balance from isotope data. *Journal of Geophysical Research*, *89*(C4), 6373–6381. https://doi.org/10.1029/JC089iC04p06373

Papritz, L. (2017). Synoptic environments and characteristics of cold air outbreaks in the Irminger Sea. *International Journal of Climatology*, *37*(S1), 193–207. https://doi.org/10.1002/joc.4991

Papritz, L., & Sodemann, H. (2018). Characterizing the local and intense water cycle during a cold air outbreak in the Nordic Seas. *Monthly Weather Review*, *146*(11), 3567–3588. https://doi.org/10.1175/MWR-D-18-0172.1

Papritz, L., & Spengler, T. (2017). A Lagrangian climatology of wintertime cold air outbreaks in the Irminger and Nordic Seas and their role in shaping air–sea heat fluxes. *Journal of Climate*, *30*(8), 2717–2737. https://doi.org/10.1175/JCLI-D-16-0605.1

Parkinson, C. L., & Cavalieri, D. J. (2008). Arctic sea ice variability and trends, 1979–2006. *Journal of Geophysical Research*, *113*(C7), C07003. https://doi.org/10.1029/2007JC004558

Pfahl, S., & Sodemann, H. (2014). What controls deuterium excess in global precipitation? *Climate of the Past*, *10*(2), 771–781. https://doi.org/10.5194/cp-10-771-2014

Pfahl, S., & Wernli, H. (2008). Air parcel trajectory analysis of stable isotopes in water vapor in the eastern Mediterranean. *Journal of Geophysical Research*, *113*(D20), D20104. https://doi.org/10.1029/2008JD009839

Pfahl, S., Wernli, H., & Yoshimura, K. (2012). The isotopic composition of precipitation from a winter storm—A case study with the limited-area model $COSMO_{iso}$. *Atmospheric Chemistry and Physics*, *12*(3), 1629–1648. https://doi.org/10.5194/acp-12-1629-2012

Pithan, F., Svensson, G., Caballero, R., Chechin, D., Cronin, T. W., Ekman, A. M., et al. (2018). Role of air-mass transformations in exchange between the Arctic and mid-latitudes. *Nature Geoscience*, *11*, 805–812. https://doi.org/10.1038/s41561-018-0234-1

Renfrew, I. A., Barrell, C., Elvidge, A. D., Brooke, J. K., Duscha, C., King, J. C., et al. (2021). An evaluation of surface meteorology and fluxes over the Iceland and Greenland Seas in ERA5 reanalysis: The impact of sea ice distribution. *Quarterly Journal of the Royal Meteorological Society*, *147*(734), 691–712. https://doi.org/10.1002/qj.3941

Renfrew, I. A., Huang, J., Semper, S., Barrell, C., Terpstra, A., Pickart, R. S., et al. (2023). Coupled atmosphere–ocean observations of a cold-air outbreak and its impact on the Iceland Sea. *Quarterly Journal of the Royal Meteorological Society*, *149*(751), 472–493. https://doi.org/10.1002/qj.4418

Renfrew, I. A., & Moore, G. W. K. (1999). An extreme cold-air outbreak over the Labrador Sea: Roll vortices and air–sea interaction. *Monthly Weather Review*, *127*(10), 2379–2394. https://doi.org/10.1175/1520-0493(1999)127<2379:aecaoo>2.0.co;2

Renfrew, I. A., Pickart, R. S., Våge, K., Moore, G. W. K., Bracegirdle, T. J., Elvidge, A. D., et al. (2019). The Iceland Greenland Seas project. *Bulletin America Meteorology Social*, *100*(9), 1795–1817. https://doi.org/10.1175/BAMS-D-18-0217.1

Schmidt, G. A., Bigg, G. R., & Rohling, E. J. (1999). Global seawater oxygen-18 database—v1.22 [Dataset]. Retrieved from https://data.giss.nasa.gov/o18data/

Semper, S., Pickart, R. S., Våge, K., Larsen, K. M. H., Hátún, H., & Hansen, B. (2020). The Iceland-Faroe Slope Jet: A conduit for dense water toward the Faroe Bank Channel overflow. *Nature Communications*, *11*(1), 5390. https://doi.org/10.1038/s41467-020-19049-5

Semper, S., Våge, K., Pickart, R. S., Valdimarsson, H., Torres, D. J., & Jónsson, S. (2019). The emergence of the North Icelandic Jet and its evolution from northeast Iceland to Denmark Strait. *Journal of Physical Oceanography*, *49*(10), 2499–2521. https://doi.org/10.1175/JPO-D-19-0088.1

Sodemann, H., Mørkved, P. T., & Wahl, S. (2023). FLIIMP—A community software for the processing, calibration, and reporting of liquid water isotope measurements on cavity-ring down spectrometers. *MethodsX*, *1*, 102297. https://doi.org/10.1016/j.mex.2023.102297

Sodemann, H., Schwierz, C., & Wernli, H. (2008). Interannual variability of Greenland winter precipitation sources: Lagrangian moisture diagnostic and North Atlantic Oscillation influence. *Journal of Geophysical Research*, *113*(D3), D03107. https://doi.org/10.1029/2007JD008503

Sodemann, H., & Touzeau, A. (2022). Iceland Greenland Seas Project (IGP): Water isotope measurements from the University of Bergen vapor isotope analyzer on board the BAS research aircraft MASIN within SNOWPACE. *NERC EDS Centre for Environmental Data Analysis*. https://doi.org/10.5285/7c8ce1c47da548a08146fa62158303c5

Sodemann, H., & Weng, Y. (2022). Iceland Greenland Seas Project (IGP): Water isotope measurements from the University of Bergen vapor isotope analyzer on board the NATO Research Vessel Alliance within SNOWPACE. *NERC EDS Centre for Environmental Data Analysis*. https://doi.org/10.5285/705abc2d9988444ba79e942f22219bc0

Sprenger, M., & Wernli, H. (2015). The LAGRANTO Lagrangian analysis tool—Version 2.0. *Geoscientific Model Development*, *8*, 1893–1943. https://doi.org/10.5194/gmdd-8-1893-2015

Tanhua, T., Olsson, K. A., & Jeansson, E. (2005). Formation of Denmark Strait overflow water and its hydro-chemical composition. *Journal of Marine Systems*, *57*(3–4), 264–288. https://doi.org/10.1016/j.jmarsys.2005.05.003

Thurnherr, I., Hartmuth, K., Jansing, L., Gehring, J., Boettcher, M., Gorodetskaya, I., et al. (2021). The role of air–sea fluxes for the water vapor isotope signals in the cold and warm sectors of extratropical cyclones over the Southern Ocean. *Weather and Climate Dynamics Discussions*, *2*, 331–357. https://doi.org/10.5194/wcd-2-331-2021

Thurnherr, I., Kozachek, A., Graf, P., Weng, Y., Bolshiyanov, D., Landwehr, S., et al. (2020). Meridional and vertical variations of the water vapor isotopic composition in the marine boundary layer over the Atlantic and Southern Ocean. *Atmospheric Chemistry and Physics*, *20*(9), 5811–5835. https://doi.org/10.5194/acp-20-5811-2020

Uemura, R., Matsui, Y., Yoshimura, K., Motoyama, H., & Yoshida, N. (2008). Evidence of deuterium excess in water vapor as an indicator of ocean surface conditions. *Journal of Geophysical Research*, *113*(D19), D19114. https://doi.org/10.1029/2008JD010209

21698996, 2024, 19, Downloaded from https://agupubs.onlinelibrary.wiley.com/doi/10.1029/2024JD041138, Wiley Online Library on [05/10/2024]. See the Terms and Conditions (https://onlinelibrary.wiley.com/terms-and-conditions) on Wiley Online Library for rules of use; OA articles are governed by the applicable Creative Commons License

Våge, K., Moore, G. W. K., Jónsson, S., & Valdimarsson, H. (2015). Water mass transformation in the Iceland Sea. *Deep Sea Research Part I: Oceanographic Research Papers*, *101*(pg), 98–109. https://doi.org/10.1016/j.dsr.2015.04.001

Våge, K., Papritz, L., Håvik, L., Spall, M. A., & Moore, G. W. K. (2018). Ocean convection linked to the recent ice edge retreat along East Greenland. *Nature Communications*, *9*(1), 1287. https://doi.org/10.1038/s41467-018-03468-6

Våge, K., Pickart, R. S., Spall, M. A., Moore, G. W. K., Valdimarsson, H., Torres, D. J., et al. (2013). Revised circulation scheme north of the Denmark Strait. *Deep Sea Research Part I: Oceanographic Research Papers*, *79*, 20–39. https://doi.org/10.1016/j.dsr.2013.05.007

Våge, K., Semper, S., Valdimarsson, H., Jónsson, S., Pickart, R. S., & Moore, G. W. K. (2022). Water mass transformation in the Iceland Sea: Contrasting two winters separated by four decades. *Deep Sea Research Part I: Oceanographic Research Papers*, *186*, 103824. https://doi.org/10.1016/j.dsr.2022.103824

Vihma, T. (2014). Effects of Arctic sea ice decline on weather and climate: A review. *Surveys in Geophysics*, *35*(5), 1175–1214. https://doi.org/10.1007/s10712-014-9284-0

Vihma, T., Pirazzini, R., Fer, I., Renfrew, I. A., Sedlar, J., Tjernström, M., et al. (2014). Advances in understanding and parameterization of small-scale physical processes in the marine Arctic climate system: A review. *Atmospheric Chemistry and Physics*, *14*(17), 9403–9450. https://doi.org/10.5194/acp-14-9403-2014

Weng, Y., Johannessen, A., & Sodemann, H. (2021). High-resolution stable isotope signature of a land-falling atmospheric river in southern Norway. *Weather and Climate Dynamics Discussions*, *2*(3), 713–737. https://doi.org/10.5194/wcd-2-713-2021

Weng, Y., Touzeau, A., & Sodemann, H. (2020). Correcting the impact of the isotope composition on the mixing ratio dependency of water vapor isotope measurements with cavity ring-down spectrometers. *Atmospheric Measurement Techniques*, *13*(6), 3167–3190. https://doi.org/10.5194/amt-13-3167-2020

Werner, M., Langebroek, P. M., Carlsen, T., Herold, M., & Lohmann, G. (2011). Stable water isotopes in the ECHAM5 general circulation model: Toward high- resolution isotope modeling on a global scale. *Journal of Geophysical Research*, *116*(D15), D15109. https://doi.org/10.1029/2011jd015681

Wernli, H., & Davies, H. C. (1997). A Lagrangian-based analysis of extratropical cyclones. I: The method and some applications. *Quarterly Journal of the Royal Meteorological Society*, *123*(538), 467–489. https://doi.org/10.1002/qj.49712353811

Woods, C., & Caballero, R. (2016). The role of moist intrusions in winter Arctic warming and sea ice decline. *Journal of Climate*, *29*(12), 4473–4485. https://doi.org/10.1175/JCLI-D-15-0773.1

Woods, C., Caballero, R., & Svensson, G. (2013). Large-scale circulation associated with moisture intrusions into the Arctic during winter. *Geophysical Research Letters*, *40*(17), 4717–4721. https://doi.org/10.1002/grl.50912

21698996, 2024, 19, Downloaded from https://agupubs.onlinelibrary.wiley.com/doi/10.1029/2024JD041138, Wiley Online Library on [05/10/2024]. See the Terms and Conditions (https://onlinelibrary.wiley.com/terms-and-conditions) on Wiley Online Library for rules of use; OA articles are governed by the applicable Creative Commons License